Pitavastatin counteracts venetoclax resistance mechanisms in acute myeloid leukemia by depleting geranylgeranyl pyrophosphate

Roberta Buono[1*], Dennis Juarez[1]*, Madhuri Paul[1]*, Sarah J. Skuli[2], Ian B. Wong[1], Ishita Tarnekar[1], Zhili Ying[1], Izabelle Le[3], Gerald Wertheim[2], A'ishah Bakayoko[2], Marisa Kruidenier[2], Said M. Sebti[4], Marina Konopleva[5], Angela G. Fleischman[6], Cholsoon Jang[3], Martin Carroll[2], David A. Fruman[1]. * equal contributions

Affiliations

[1] Department of Molecular Biology & Biochemistry, University of California Irvine, Irvine, CA, 92697, USA; [2] Department of Medicine, Division of Hematology & Oncology, University of Pennsylvania, Philadelphia, PA 19104, USA; [3] Department of Biological Chemistry, Center for Epigenetics and Metabolism, Department of Chemistry, University of California Irvine, Irvine, CA, 92697, USA; [4] Department of Pharmacology and Toxicology and Massey Comprehensive Cancer Center, Virginia Commonwealth University, Richmond, VA, 23298, USA; [5] Albert Einstein Colege of Medicine, Montefiore Einstein Comprehensive Cancer Center, 1300 Morris Park Ave, Bronx, NY, 10461, USA; [6] Division of Hematology-Oncology, Department of Medicine, University of California Irvine, Irvine, CA, 92697, USA.

Address Correspondence:

David A. Fruman, PhD, UC Irvine, 839 Health Sciences Road, 216 Sprague Hall, Irvine, CA, 92697-3905. dfruman@uci.edu

or

Roberta Buono, PhD, UC Irvine, 839 Health Sciences Road, 216 Sprague Hall, Irvine, CA, 92697-3905. buonor@uci.edu

Character Count: Abstract, 1525; Introduction, 5632; Results, 17293; Discussion, 9777; Methods, 16,453; Figure Legends, 5852. Total = 56,532

Abstract

The BCL2 inhibitor venetoclax has therapeutic activity in several hematological malignancies. In acute myeloid leukemia (AML), venetoclax combined with hypomethylating agents is the standard of care for patients unfit for intensive chemotherapy, but intrinsic and acquired resistance are common. Loss of p53 function is strongly associated with venetoclax resistance, and adding venetoclax to 5-azacitidine provides no overall survival benefit in *TP53*-mutant AML. Other frequent mechanisms of venetoclax resistance in AML include *FLT3* mutations, MCL-1 upregulation, and altered mitochondrial metabolism. Unfortunately, it has been challenging to develop agents that target these mechanisms directly and combinatorially. Here we report that pitavastatin, an inhibitor of HMG-CoA-reductase, promotes apoptosis and overcomes several venetoclax resistance mechanisms in human AML cells. At clinically achievable concentrations, pitavastatin treatment has potent cytotoxic activity in cells with mutations in *TP53* or *FLT3*. The apoptotic mechanism involves p53-independent PUMA upregulation and reduced MCL-1 expression. Pitavastatin also suppresses mitochondrial gene expression and oxidative metabolism. The pro-apoptotic actions of pitavastatin depend on depletion of geranylgeranyl pyrophosphate (GGPP) and can be recapitulated by inhibiting GGPP synthase or geranylgeranyltransferase-1 enzymes. These results provide a mechanistic rationale for adding pitavastatin to AML regimens to prevent or overcome venetoclax resistance.

Keywords

Leukemia/apoptosis/venetoclax/statin/drug resistance

Introduction

B cell lymphoma 2 (BCL2) is an oncoprotein and a member of a family of apoptosis-regulating proteins (Cory *et al*, 2016). The pro-survival family members (BCL2, BCL-xL, MCL-1, BCL-w, BFL-1) contain four domains with homology to BCL2 (BH1, BH2, BH3, BH4 domains). Levels of these proteins are often elevated in blood cancer cells to escape stress-induced increases of pro-apoptotic proteins, including "BH3-only" proteins such as BIM and PUMA (Cory *et al*, 2016; Leverson *et al*, 2017; Merino *et al*, 2018; Valentin *et al*, 2018). BH3 mimetics are cell-permeable small molecules that block the BH3-binding pocket of BCL2 family members, inhibiting their pro-survival function and promoting apoptosis (Cory *et al*, 2016; Leverson *et al*, 2017; Merino *et al*, 2018; Valentin *et al*, 2018). Their clinical utility is validated by BCL2-selective venetoclax (ABT-199) regimens for front-line treatment of chronic lymphocytic leukemia (CLL) and acute myeloid leukemia (AML) (Roberts *et al*, 2016; DiNardo *et al*, 2019). However, there remains a critical need to identify combinations that further broaden and deepen responses to venetoclax and prevent the emergence of resistance (Bose *et al*, 2017; Grant, 2017).

AML demonstrates diverse resistance mechanisms to BCL2 inhibition. Despite the unquestionable success in the treatment of *TP53*-mutant CLL (Roberts *et al*, 2016), subsequent basic and clinical studies highlight that bi-allelic *TP53* loss is a frequent mechanism of resistance in AML (Nechiporuk *et al*, 2019; DiNardo *et al*, 2020b; Thijssen *et al*, 2021). Indeed, while venetoclax combined with 5-azacitidine (AZA) extends survival in AML patients unfit for intensive chemotherapy (DiNardo *et al*, 2020a), this combination provides no overall survival benefit compared to AZA alone in patients with *TP53* loss (Pollyea *et al*, 2022; Döhner *et al*, 2024). Other factors associated with venetoclax resistance in AML include reduced

mitochondrial priming through upregulation of other anti-apoptotic proteins such as MCL-1 (Bhatt *et al*, 2020), certain genetic drivers (e.g., *FLT3*-internal tandem duplication (ITD) and *RAS*; (DiNardo *et al*, 2020b; Sango *et al*, 2024)), *BCL2* mutations (Brown *et al*, 2025), and altered mitochondrial dynamics including translation, respiration and mitophagy (Sharon *et al*, 2019; Liu *et al*, 2020; Bosc *et al*, 2021; Glytsou *et al*, 2023).

The mevalonate pathway is a targetable cancer dependency that supports proliferation and survival (Mullen *et al*, 2016; Juarez & Fruman, 2021). Many oncogenes increase cellular demand for mevalonate pathway outputs, while driving mevalonate flux by increasing expression of HMG-CoA-reductase (HMGCR) or other pathway enzymes (Juarez & Fruman, 2021). This has spurred interest in repurposing statins (selective HMGCR inhibitors) for oncology (Clendening & Penn, 2012; Longo *et al*, 2020; Juarez & Fruman, 2021; Tripathi *et al*, 2024). We reported that statins promote apoptosis and sensitize to venetoclax in blood cancer cell lines and primary cells (Lee *et al*, 2018; Juarez *et al*, 2023), a finding independently validated by others (Gimenez *et al*, 2020; Al-Zebeeby *et al*, 2019). Our retrospective analysis of venetoclax clinical trials revealed that statin use is associated with significantly increased rates of complete response in CLL or multiple myeloma (MM) (Lee *et al*, 2018; Juarez *et al*, 2023). These findings provided rationale for a prospective phase 1 clinical trial (clinicaltrials.gov identifier NCT04512105) testing pitavastatin in combination with venetoclax in AML and CLL. This trial found that the addition of pitavastatin to venetoclax regimens is tolerable (Brem *et al*, 2024).

The barriers that have limited the clinical translation of statins as oncology drugs are the many niche mechanisms of action described in the literature and the underappreciated role of statin pharmacology in design of clinical trials (Abdullah *et al*, 2018; Juarez & Fruman, 2021). We have previously determined that the pro-apoptotic effect of statins is due to depletion of

cellular pools of geranylgeranyl pyrophosphate (GGPP) (Lee *et al*, 2018; Juarez *et al*, 2023), the isoprenoid substrate for protein geranylgeranylation, and this finding is generalizable to several of the described mechanisms of statin's anti-cancer effects (Juarez & Fruman, 2021; Wang & Casey, 2016). Concerning statin pharmacology, we found that pitavastatin has approximately 3-fold greater potency than other statins in cell-based assays, and acts at clinically achievable concentrations to block geranylgeranylation and promotes apoptosis in MM cells (Juarez *et al*, 2023). Pitavastatin in our phase I trial also demonstrated preliminary signs of efficacy with all subjects achieving complete remission (Brem *et al*, 2024).

Here we leverage our prior findings to assess statin efficacy against AML venetoclax resistance using cell line models and primary cells. To focus on mevalonate pathway outputs relevant to survival signaling in AML cells, we identify cellular responses that are induced by pitavastatin in a manner dependent on GGPP depletion and are recapitulated by geranylgeranyltransferase-1 (GGTase-1) inhibitors. These analyses revealed that pitavastatin sensitizes to venetoclax via p53-independent upregulation of PUMA and by rewiring cellular transcription to disrupt mitochondrial gene expression and metabolism. In a subset of AML cells, pitavastatin diminishes the expression of MCL-1. Together, these results show that pitavastatin can overcome several common mechanisms of venetoclax resistance in AML and should be assessed in combination with venetoclax and AZA in future AML clinical trials.

Results

Pitavastatin induces p53-independent cytotoxicity at sub-micromolar concentrations in AML cells

Previously we reported that simvastatin sensitizes AML cell lines and a subset of primary AML samples to venetoclax cytotoxicity (Lee *et al*, 2018), and that pitavastatin is cytotoxic in MM cell lines at lower concentrations than simvastatin (Juarez *et al*, 2023). Here we tested pitavastatin in a panel of AML cell lines with different genetic lesions (Table EV1). Cytotoxicity assays demonstrated that 48-hour treatment with pitavastatin concentrations as low as 300 nM reduced viability in OCI-AML3 and HNT-34 cells and enhanced the weak cytotoxic effect of venetoclax (Figure 1A). A similar effect was observed in MV4-11 cells at 1 μM pitavastatin (Figure 1A). The mechanism by which pitavastatin enhanced cytotoxicity was caspase-dependent, as it was blocked by the inhibitor Q-VD-OPh at 24hr (Fig. EV1A). In the MOLM13 and PL-21 cell lines, pitavastatin alone had minimal cytotoxic activity but enhanced the effect of venetoclax (Figure 1A). Pitavastatin retained cytotoxicity in a venetoclax-resistant subline of MOLM13 (Han *et al*, 2020) (Fig. EV1B). The combination of pitavastatin and venetoclax was synergistic in OCI-AML3, HNT-34, MV4-11, and MOLM13 cells (Table EV2; the latter three cell lines have *FLT*3-ITD). We identified a pitavastatin-resistant AML cell line (OCI-M1) (Figure 1A, Table EV2) that we used as a comparator for mechanistic studies. Consistent with prior publications (Lee *et al*, 2018), simvastatin enhanced venetoclax cytotoxicity but only at concentrations above 1 μM in OCI-AML3 and MOLM13 cells (Fig. EV1C).

We extended these studies to cultures of primary AML cells obtained from cryopreserved adult AML mononuclear specimens (Table EV3). Primary cultures were noted to be more pitavastatin sensitive than established cell lines with notable cytotoxicity at 100 – 300 nM including three samples with *TP53* mutations and three out of five samples with *FLT3*-ITD (Figure 1B and EV2A, B, C). Venetoclax further enhanced the killing of several of the primary AML samples (Figure 1B). In addition, pitavastatin increased cytotoxicity of the combination of

venetoclax and AZA in several primary AML samples (Fig. EV2C). In most of these samples, the combination of venetoclax plus pitavastatin was more effective than venetoclax plus AZA.

We showed previously that expression of a dominant-negative p53 did not affect simvastatin-mediated cytotoxicity or venetoclax sensitization in OCI-AML3 cells, whereas effects of the chemotherapy drug etoposide were abrogated (Lee *et al*, 2018). To investigate further the relationship of p53 status to pitavastatin sensitivity, we used isogenic MOLM14 cell lines with either wild-type or bi-allelic deletion of *TP53*, generated by CRISPR/Cas9 (Skuli *et al*, 2025). In parental MOLM14 cells, pitavastatin in the 1-3 μM concentration range was sufficient to promote cell death (Fig. EV3). The p53-deficient MOLM14 variants, which are resistant to cytarabine (Skuli *et al*, 2025) and less sensitive than control MOLM14 cells to venetoclax (Fig. EV3), remained sensitive to pitavastatin and to the synergistic or additive cytotoxicity of pitavastatin plus venetoclax (Fig. EV3, Table EV4).

Overall, the findings that pitavastatin at submicromolar concentrations (clinically achievable with FDA-approved doses; (Catapano, 2012; Luo *et al*, 2015)), enhances the cytotoxic activity of venetoclax in a variety of AML cell lines and primary cells, and that primary AML cells are more sensitive to pitavastatin at lower concentrations than AML cell lines, suggest that addition of pitavastatin to venetoclax regimens in AML may be a feasible approach for treatment, including in cases with p53 inactivation or *FLT3*-ITD.

Pitavastatin alters expression of BCL2 family members PUMA and MCL-1

p53-independent upregulation of PUMA is a general mechanism by which statins sensitize blood cancer cells to BH3 mimetics (Lee *et al*, 2018; Juarez *et al*, 2023). Consistent with our previous findings, pitavastatin treatment increased expression of PUMA protein in OCI-AML3,

HNT-34 and MV4-11 cell lines that are sensitive to statin cytotoxicity (S4A, B, C). Pitavastatin treatment caused lesser or no PUMA upregulation in cell lines that are less sensitive (MOLM-13, PL-21) or resistant to cytotoxicity (OCI-M1) (Fig. EV4A, B, D), supporting the correlation of PUMA induction and cytotoxicity. Additionally, in our isogenic *TP53* deleted MOLM14 cells, pitavastatin induced PUMA expression to a comparable degree in control (Fig. EV5A). CRISPR/Cas9-mediated knockout of the *BBC3* gene encoding PUMA (Fig. EV5B, C) partially reversed the cytotoxic effect of pitavastatin in OCI-AML3 and MOLM-14 cells but not in MOLM-13 cells (Figure 2A).

Increased expression of and dependence on MCL-1 can confer venetoclax resistance in AML cells (Teh *et al*, 2017; Caenepeel *et al*, 2018). We assessed how venetoclax and pitavastatin co-treatment affects protein expression of PUMA and MCL1. In OCI-AML3, MOLM13, and MOLM14 cells, pitavastatin reduced expression of MCL-1 and/or prevented the increase in MCL-1 following venetoclax treatment (Fig. EV6A, B). In general, the combination of pitavastatin with venetoclax reduced MCL-1 expression more than pitavastatin alone. We also noted that in some AML cell lines, venetoclax reduced PUMA expression and suppressed PUMA upregulation by pitavastatin (Fig. EV6A, B). In the venetoclax-resistant MOLM13 subline, pitavastatin increased low basal PUMA expression but did not reduce the high basal MCL-1 expression (Fig. EV6C). In two of the three *TP53* mutant primary AML cells we tested, 24hr treatment with pitavastatin reduced MCL-1 or increased PUMA expression (Fig. EV6D). Thus, pitavastatin can alter the balance of pro- and anti-apoptotic BCL2 family members via at least two mechanisms.

Pitavastatin increases cytotoxicity and PUMA expression via depletion of GGPP and inhibition of geranylgeranylation

In most blood cancer cell models, statin cytotoxicity is linked to depletion of isoprenoid intermediates downstream of mevalonate (Xia *et al*, 2001; Wong *et al*, 2007). Using an antibody that detects the unprenylated form of RAP1A GTPase, we found that pitavastatin inhibited geranylgeranylation at 1 μM or lower concentrations in all cell lines except OCI-M1 (Figure 2B, D and EV4C, D). In addition, supplementing culture medium with excess GGPP prevented pitavastatin-induced PUMA expression (Figure 2B, C) and cytotoxicity in statin-sensitive cells (Fig. EV7A). This result suggests that GGPP depletion is required for the pitavastatin mechanism of action. To determine whether GGPP-depletion is sufficient, we used an inhibitor of GGPP synthase (THZ145; (Xia *et al*, 2018)) and found that it had cytotoxic activity in OCI-AML3 cells and increased PUMA expression to a similar extent as pitavastatin (Fig. EV7B, C).

We showed previously that a GGTase-I inhibitor, GGTI-298, increased PUMA in AML cells (Lee *et al*, 2018). Unexpectedly, while GGTI-298 upregulated PUMA, had cytotoxic activity, and sensitized to venetoclax, the structurally related GGTI-2133 had minimal effects on these functional readouts (Figures 2D, E and EV7B, C). GGTI-2133 had equivalent or greater ability to reduce prenylation of RAP1A, a commonly used readout of GGTase-1 activity (Figure 2D and EV7B). Furthermore, both compounds reduced actin polymerization, which is driven by GTPases such as RHO, RAC and CDC42 known to be substrates of GGTase-1 (Wang & Casey, 2016; Juarez & Fruman, 2021) (Fig. EV8A). While GGTI-2133 and GGTI-298 both have observed activity on inhibition of GGTase-I substrates, GGTI-298 more closely phenocopies the anti-cancer effects of pitavastatin on AML cell function making GGTI-2133 an interesting comparator for further study. It is unlikely that the effects of GGTI-298 are simply due to off-

target activity on farnesyltransferases or other enzymes, given that GGPP synthase inhibition had cytotoxic activity similar to statins. Moreover, a more selective and potent GGTase-1 inhibitor (GGTI-2417; (Peng *et al*, 2006)) exerted cytotoxic activity in AML cell lines and increased PUMA expression and unprenylated RAP1A (Fig. EV8B-D). Together these data support the conclusion that GGTase-1 is a key prenyltransferase mediating pro-survival activities of GGPP in AML cell lines.

Pitavastatin and GGTI-298 elicit widespread transcriptome changes including enhanced apoptotic gene signatures

A challenge to applying transcriptome studies to decipher statin cytotoxic mechanism is that there are multiple outputs of the mevalonate pathway, of which only some play key roles in cell survival regulation. Our observation that GGTI-298 and GGTI-2133 have partially distinct activities allowed a novel approach to distinguishing the most relevant gene expression changes associated with cell death sensitization. Specifically, we reasoned that differentially expressed genes (DEGs) shared in pitavastatin and GGTI-298 treatment conditions but not after GGTI-2133 treatment are most relevant to the cytotoxic mechanism. In accord, we treated OCI-AML3 and HNT-34 cells with vehicle alone (0.1% DMSO) or pitavastatin (PIT; 1 μM) or GGTIs (10 μM) and harvested RNA for bulk RNA sequencing. We chose a time point (16hr) before the onset of apoptosis but when PUMA upregulation is robust at the protein level.

Pitavastatin and GGTI-298 each caused broad changes in gene expression (vs. vehicle condition, Supplementary Excel File 1) with a high degree of overlap in both OCI-AML3 (Figure 3A) and HNT-34 (Fig. EV9A). GGTI-2133 treatment altered expression of many fewer genes in both cell lines (Figure 3A and EV9A, Supplementary Excel File 1). Principal

component analysis (PCA) supported the similarity of cells treated with GGTI-2133 or vehicle alone (Fig. EV9B). In accord, unbiased transcriptome-wide analysis of rlog-based sample distances demonstrated clustering of vehicle with GGTI-2133 and of PIT with GGTI-298 in both OCI-AML3 and HNT-34 (Fig. EV9C). Gene set enrichment analysis (GSEA) for Hallmark and Reactome pathways in OCI-AML3 cells showed several shared responses to pitavastatin and GGTI-298, including reduced expression of MYC and E2F targets and an increase in genes associated with apoptosis (Figure 3B). Similar gene sets were identified in HNT-34 cells, which also displayed a signature of cholesterol homeostasis and SREBP targets suggesting a stronger feedback response (Figure 3B). The *SREBF2* mRNA was increased by both pitavastatin and GGTI-298, but not GGTI-2133, with a greater effect in HNT-34 cells (Fig. EV10). In agreement with the increase PUMA protein expression, the *BBC3* gene encoding PUMA was significantly upregulated by pitavastatin and GGTI-298, but not GGTI-2133, in both cell lines (Fig. EV10).

An independent approach using Ingenuity Pathway Analysis software also identified MYC/E2F downregulation and PUMA upregulation, along with c-JUN upregulation, as cellular mechanisms induced by pitavastatin and GGTI-298 (Fig. EV9D).

Transcriptome analysis of pitavastatin effects dependent on GGPP depletion

As a second approach to defining statin cytotoxic mechanism, we determined which gene expression changes induced by pitavastatin are dependent on GGPP depletion. We conducted bulk RNA sequencing on OCI-AML3 cells treated for 16hr with vehicle alone (0.1% DMSO), pitavastatin (PIT; 1 μM), GGPP (5 μg/ml) or PIT + GGPP. Compared to vehicle-treated samples, there were ~1400 DEGs in the PIT-treated condition but only 129 in the GGPP condition and 103 in the PIT+GGPP condition (Figure 4A). Applying a $\log_2$ fold-change (LFC) cut-off of +/- 0.1,

there were only three DEGs in the PIT+GGPP vs. Vehicle condition and one in the GGPP vs. Vehicle (Supplementary Excel File 2). PCA showed that PIT-treated samples clustered together and distant from the other three groups (Fig. EV11A). These data indicate that statin-mediated transcriptional reprogramming at 16hr is almost entirely dependent on GGPP depletion. In MOLM13 cells, which are less pitavastatin sensitive than OCI-AML3 cells (Figure 1), pitavastatin caused many fewer DEGs yet these were still largely dependent on GGPP depletion (add EV11B). Hallmark GSEA analysis of OCI-AML3 cells showed downregulation of MYC and E2F targets (Figure 4B), consistent with the first transcriptome experiment.

Functional validation of transcription factor targets

To investigate the mechanism of reduced MYC target gene expression, we measured changes in MYC protein by western blot. Treatment of OCI-AML3 cells with pitavastatin reduced MYC expression, an effect that was reversed by mevalonate or GGPP and phenocopied by GGTI-298 and GGTI-2417, but not GGTI-2133 (Figure 5A, B; EV12). Pitavastatin also reduced MYC protein amounts in primary AML samples UCI-01 and UCI-06 (Figure 5A). MYC protein downregulation was not observed in PL-21 cells (resistant to pitavastatin single-agent cytotoxicity) but was also minimal in HNT-34 cells (sensitive to pitavastatin cytotoxicity) (Figure 5A, B).

Downregulation of MYC and E2F is commonly observed under conditions of cell cycle arrest (Schuldiner & Benvenisty, 2001; Baudino *et al*, 2003). Accordingly, we found that pitavastatin and GGTI-298, but not GGTI-2133, increased the proportion of cells in G1 and decreased S phase in OCI-AML3 cells (Figure 5C). Pitavastatin and GGTI-298 had minimal

effects on cell cycle in HNT-34 cells (Figure 5C) in alignment with the preservation of MYC protein expression (Figure 5A).

Pitavastatin strongly increased expression of the *TSC22D3* gene, with similar induction by GGTI-298 but to a lesser extent by GGTI-2133 (EV10). *TSC22D3* gene encodes the glucocorticoid-induced leucine zipper (GILZ) protein that contributes to dexamethasone-induced apoptosis in MM cells (Kervoëlen *et al*, 2015). In accord with mRNA changes, protein measurements by western blot showed that pitavastatin increased GILZ expression in statin-sensitive cell lines but not in resistant PL-21 cells (Figure 5A, B). Addition of GGPP prevented the pitavastatin-induced GILZ expression (Fig. EV13A). However, CRISPR/Cas9-mediated deletion of GILZ in OCI-AML3 cells did not affect cell viability changes in response to pitavastatin alone or the combination with venetoclax (Fig. EV13B, C). These data suggest that GILZ induction is not essential for statin cytotoxicity.

Pitavastatin suppresses oxidative metabolism and TCA cycle in OCI-AML3 cells

GSEA analysis showed that pitavastatin and/or GGTI-298 reduced gene sets associated with mitochondrial protein import and oxidative phosphorylation (Figure 3C, 4B). Combined analysis of data from OCI-AML3 cells in both transcriptome studies identified a set of 85 shared DEGs representing nuclear-encoded mitochondrial genes, of which only 3 were significantly changed by GGTI-2133 (Fig. 6A). A large majority of these (70) were downregulated, including genes whose products regulate the function of components of the electronic transport chain (*CYCS*, *DHODH*, *NDUFAF4*, *TIMM21*, *TMEM126B*, *TMEM177*). The smaller subset of upregulated mitochondrial genes included *BBC3* (Fiogure 6A).

The changes in expression of mRNAs encoding mitochondrial proteins prompted us to assess mitochondrial mass and function. Flow cytometry demonstrated reduced TOM20 expression after pitavastatin treatment in OCI-AML3 cells but not MOLM13 cells (Fig. EV14A). As alternate assays for mitochondrial mass we used quantitative PCR to measure the ratio of mitochondrial to genomic DNA and flow cytometry to determine the amount of cardiolipin, a mitochondrial-specific phospholipid. While the DNA assays indicated reduced mitochondrial mass in OCI-AML3 cells treated with pitavastatin (Fig. EV14B), similar to the TOM20 measurements (Fig. EV14A), the cardiolipin assay did not confirm this finding (Fig. EV14C). Using a Seahorse metabolic flux analyzer to measure the oxygen consumption rate (OCR), we found that pitavastatin reduced basal oxygen consumption in OCI-AML3 cells but not in MOLM13 cells (Figure 6B, C), consistent with the lack of downregulation of mitochondrial genes in MOLM13. Addition of GGPP partially reversed the decreased basal OCR in OCI-AML3 cells treated with pitavastatin (Figure 6D). The combination of pitavastatin with venetoclax strongly and significantly reduced basal OCR and spare respiratory capacity in OCI-AML3 and MOLM13 cells (Fig. EV15A, B). However, after 16hr of treatment with venetoclax +/- pitavastatin, a large percentage of cells had released cytochrome C (Fig. EV15C, D), effects that might indirectly suppress OCR. Cytochrome C release did not occur with pitavastatin alone (Fig. EV15C), a condition where basal OCR was reduced in OCI-AML3 cells (Figure 6B, C). Concurrent with decreased OCR, pitavastatin also caused loss of mitochondrial membrane potential in a significant percentage of OCI-AML3, as well as MOLM14 parental and *TP53* mutant lines (Fig. EV16A, B).

To investigate whether mitochondrial dysfunction is associated with metabolic flux, we conducted untargeted metabolomics combined with [U-^{13}C]-glucose tracing. The data revealed

that, in OCI-AML3 cells, 16-hour pitavastatin treatment significantly reduced the production of TCA cycle intermediates (citric acid, α-ketoglutarate, fumarate, malate) from glucose (Figure 6E).

Discussion

The combination of venetoclax with 5-azacitidine (VEN-AZA) is a standard of care regimen for AML patients who are >75 years old or unfit for intensive chemotherapy. As first-line therapy in previously untreated AML patients, VEN-AZA increases the frequency of complete remission and provides an increase in median OS to (14.7) months compared to (9.6) months with AZA alone (DiNardo *et al*, 2020a). However, it has become clear that VEN-AZA provides no survival advantage compared to AZA alone in the subgroup with *TP53* loss of function (Pollyea *et al*, 2022; Döhner *et al*, 2024). In addition, venetoclax resistance is common in AML cases with *FLT3*-ITD and/or *RAS* mutations, enhanced mitochondrial metabolism, or MCL-1 overexpression (DiNardo *et al*, 2020b; Bhatt *et al*, 2020; Bosc *et al*, 2021; Sango *et al*, 2024). Currently there are no clinically used drugs that can address multiple venetoclax resistance mechanisms. Magrolimab, a CD47 blocking antibody that showed promise in early trials, showed no benefit in randomized phase 3 trials when combined with VEN-AZA in untreated AML or with AZA in *TP53*-mutated AML (Daver *et al*, 2025)(Zeidner *et al*, 2025) . Here we show that an FDA-approved HMG-CoA-reductase inhibitor, pitavastatin, potentiates venetoclax cytotoxicity in multiple AML cell models including established and primary AML cells with *TP53* mutations or *FLT3*-ITD. In most statin-sensitive cell lines, pitavastatin upregulates the pro-apoptotic protein PUMA. In some cell lines, pitavastatin decreases MCL-1, and can inhibit oxidative metabolism.

The selective cytotoxicity of statins in AML compared to normal hematopoietic progenitors was first reported more than 30 years ago (Newman *et al*, 1994). Why has this not yet led to application in clinical practice? Three reasons deserve prominent attention. First, the great majority of cell-based assays in the literature employ concentrations of statins (5-20 μM) that are 100 – 1000 times higher than clinical achievable by the statin drugs most prescribed (i.e., simvastatin, atorvastatin, rosuvastatin). Thus, the cytotoxic effects and mechanisms described *in vitro* have questionable relevance to the clinical scenario. Second, it is essential to choose hydrophobic statin drugs with good bioavailability (Abdullah *et al*, 2018). Some prospective AML clinical trials have used hydrophilic statins (e.g., pravastatin; (Kornblau *et al*, 2007; Advani *et al*, 2018)) that, even at high doses, do not readily enter blood cells that lack active transport mechanisms present in hepatocytes. Third, statin pharmacology is different in rodents (Schonewille *et al*, 2016), resulting in inadequate inhibition of the mevalonate pathway and thus generally weak *in vivo* anti-cancer effects in preclinical models (Hillis *et al*, 2024; Skuli *et al*, 2025), which can diminish enthusiasm for advancing to human trials.

Pitavastatin has gained recognition as an ideal molecule for applications in oncology (Abdullah *et al*, 2018) and to ameliorate adverse cardiac events in HIV patients (Grinspoon *et al*, 2023). This compound is ~3-times more potent on a molar basis in cell lines, achieves plasma concentrations in the 200 – 500 nM range in humans at the FDA-approved dose, and has an extended half-life and fewer drug interactions than other statins (Catapano, 2010, 2012; Juarez & Fruman, 2021; Juarez *et al*, 2023). Our phase 1 clinical trial found that daily 2 or 4 mg doses of pitavastatin were well tolerated in AML and CLL patients receiving venetoclax as standard of care (Brem *et al*, 2024). In this study, we show that pitavastatin is more potent than simvastatin in AML cell lines. While the concentration of pitavastatin that has single-agent cytotoxicity

varies among AML cell lines from 0.3 to 3 μM, we observe activity in primary AML cells at concentrations in the 0.1 – 0.3 μM range. Importantly, pitavastatin is active in *TP53*-mutant samples regardless of their sensitivity to VEN or AZA. Pitavastatin enhanced venetoclax cytotoxicity in four AML cell lines with FLT3-ITD (MOLM13, MOLM14, MV4.11, PL-21) and in three out of five primary samples tested (UCI-03, -07 and -09). Notably, pitavastatin even partially overcomes venetoclax resistance in a MOLM13 cell model.

Selective inhibition of BCL2 with venetoclax is most effective in cancers that depend on BCL2 for survival. Basal or acquired dependence on MCL-1 is a common mechanism of venetoclax resistance in AML (Teh *et al*, 2017; Moujalled *et al*, 2019; Zhang *et al*, 2022). Unfortunately, direct targeting of MCL-1 with highly selective compounds is associated with significant adverse events (Desai *et al*, 2024). Suppressing MCL-1 transcription via CDK9 inhibitors is another strategy under investigation (Davids *et al*, 2025). Pitavastatin is an alternative option, based on our observation that the compound can overcome venetoclax-induced increases in MCL-1 expression. In these experiments, we observed that in several AML cell lines, treatment with venetoclax or the combination of pitavastatin with venetoclax reduced PUMA protein amounts compared to basal. Thus, the mechanisms of cytotoxicity may differ in response to pitavastatin alone versus the combination with venetoclax. In the clinical setting, both single agent and combination mechanisms may contribute to efficacy as the plasma concentrations of each drug change over time.

There has been considerable interest in targeting oxidative metabolism to treat AML. Preclinical studies established that AML cell venetoclax resistance correlates with increased mitochondrial metabolism (Liu *et al*, 2020; Bosc *et al*, 2021; Grenier *et al*, 2022). Furthermore, various OXPHOS inhibitors potentiate cytotoxicity of venetoclax and prevent or overcome

resistance (Liu *et al*, 2020; Bosc *et al*, 2021; Hua *et al*, 2023; Velez *et al*, 2016). A selective inhibitor of complex-1 of the electron transport chain, IACS-010759, entered clinical trials but a phase I study reported significant toxicities and lack of efficacy at tolerated doses (Molina *et al*, 2018; Yap *et al*, 2023). Treatment with pitavastatin might provide an alternative, well-tolerated route to achieve a reduction in mitochondrial respiration. Our data show that at a time point before the onset of apoptosis, pitavastatin reduces basal OCR while triggering MMP loss in a significant fraction of cells. In OCI-AML3 cells, these mitochondrial defects were accompanied by decreased flux of glucose to the TCA cycle. In a separate paper, we reported that pitavastatin and rosuvastatin reverse the increase in OXPHOS observed in cytarabine-resistant *TP53*-mutant AML cells (Skuli *et al*, 2025). Mitochondrial dysfunction has the potential to reduce ATP production and cause activation of AMPK, a pathway that can promote PUMA expression via the integrated stress response (ISR) in AML cells (Grenier *et al*, 2022). We previously showed that pitavastatin activates the ISR in MM cell lines; however, under the same conditions a chemical inhibitor of the ISR did not affect statin cytotoxicity or venetoclax sensitization in AML cell lines (Juarez *et al*, 2023).

The effects of pitavastatin on AML cell survival, PUMA upregulation, and OXPHOS are dependent on GGPP depletion as they are largely rescued by exogenous GGPP. Furthermore, two inhibitors of GGTase-1 (GGTI-298 and GGTI-2417) recapitulated many actions of pitavastatin, supporting the hypothesis that GGTase-1 substrates have essential functions in AML cell survival. A key question is how the mevalonate/GGPP axis programs AML transcription to promote proliferation and survival. To address this, we determined which transcriptional changes induced by pitavastatin are recapitulated by GGTI-298 and reversed by GGPP. Together these transcriptome analyses revealed several novel findings. First, the mevalonate pathway via GGPP

promotes expression of cMYC and E2F target genes, correlating with cell cycle progression. Second, the mevalonate pathway regulates expression of many nuclear-encoded mitochondrial genes, some which are associated with OXPHOS and the TCA cycle. This connection might underly how treatment with pitavastatin reduces basal OCR and spare respiratory capacity and disrupts MMP. Notably, the extent of pitavastatin-induced transcriptional reprogramming is quite variable, with more prominent effects in OCI-AML3 cells compared to other lines tested here (need Supplementary Tables with volcano plots). This might be due in part to varying levels of positive feedback reactivation of the mevalonate pathway (Pandyra *et al*, 2014); indeed, pitavastatin-treated HNT-34 cells had a strong cholesterol pathway upregulation signature and overall fewer DEGs than OCI-AML3 cells (Fig. 3B, EV9A, EV10B). It is possible that the kinetics of transcriptional reprogramming differs among cell lines such that a shared DEG signature is difficult to define. Ongoing work aims to (1) identify transcription factors or epigenetic changes underlying altered gene expression and (2) determine which geranylgeranylated protiens transmit key survival signals that are disrupted by statin treatment.

To broaden the utility of venetoclax to improve outcomes in AML, it is essential to identify new combination regimens that address common mechanisms of resistance. In this study we have presented evidence that pitavastatin, an FDA-approved agent, has potent cytotoxic activity in human AML cells including samples with *TP53* loss. Pitavastatin treatment achieves several cellular changes that sensitize to venetoclax including PUMA upregulation, MCL-1 downregulation, and reduced respiration. Together with other findings from various laboratories (Gimenez *et al*, 2020; Al-Zebeeby *et al*, 2019; Abdullah *et al*, 2018), these results support further investigation of pitavastatin/venetoclax combinations in AML.

Methods

Chemicals

Pitavastatin (Fisher Scientific #NC0110176), venetoclax (Selleck Chemicals #S8048), S63845 (Selleck S8383/Chemgood C-1370), GGTI-298 (Fisher Scientific # HY-15871), GGTI-2133 (Sigma Aldrich #G5294), THZ145 (MedChem Express #HY-150168) and GGTI2417 (synthesized as described (Peng *et al*, 2006)) were dissolved in DMSO. Mevalonate (Sigma-Aldrich #90469) was resuspended with a 7:3 solution of methanol and 10 mM ammonium hydroxide. GGPP (Sigma #G6025-1VL or Cayman Chemical 63330) and FPP (Cayman Chemical #63250) were used at 5 µg/ml.

Cell Culture

Cell lines were obtained from commercial repositories (ATCC or DSMZ) and authenticated annually through STR profiling using the University of Arizona Genomics Core. MOLM13 parental and venetoclax resistant were described previously (Han *et al*, 2020). Cell lines were tested for mycoplasma infection annually. Unless otherwise noted, cell lines used in the study were maintained in RPMI-1640, 10% FBS, 1% penicillin-streptomycin-glutamine (Gibco # 10-378-016) and 10 mM HEPES (Corning #25-060-CI). Cell lines were maintained at concentrations between 0.5 million to 2 million per ml. Experiments requiring incubation times less than 24 hours were plated at 1 million per ml while greater than 24 hours were plated at 0.5 million per ml. MOLM14 parental cells and *TP53* mutant were kindly provided by our collaborator Dr. Sara Skuli and cultured in alphaMEM supplemented with 10% FBS.

Human cells were provided by UCI biobank or U-Penn and cultured in IMDM supplemented with 15% BIT 9500 (Stemcells Technologies #09500), and human SCF (Peprotech #300-07) 100

ng/ml, human Flt3-Ligand (Peprotech #300-19) 50 ng/ml, human IL-3 (Peprotech #200-03) 20 ng/ml, human G-CSF (Peprotech #300-23) 20 ng/ml, 1:100 penicillin-streptomycin-glutamine, beta mercaptoethanol and StemRegenin 1 (Stemcells Technologies #72342) 1 μM.

Cell Viability

Cell viability assays were performed in 96-well format for 48 hours. Briefly, 5 x 10^4 cells were cultured in 200 μL growth medium with inhibitors for 48 hours. Inhibitors did not exceed a 0.1% DMSO concentration. Viability was determined by fluorescence of propidium iodide (Life Technologies #P3566) and/or Annexin V Alexa Fluor 647 conjugate (Life Technologies #A23204) measured by the Novocyte 3000 (Agilent) or Attune NxT (Thermo Fisher). Viability of cells was quantified using FlowJo software v10.10.0 (FlowJo LLC).

Cell Cycle Analysis

After 48h treatment cells were harvested and washed in PBS with 5 mM EDTA, then fixed in cold ethanol for 30min at room temperature. Cells were spun down, washed and treated with ribonuclease for 30min at 37°C. Cells were stained with propidium iodide, and 10,000 cellular events were collected by flow cytometry using Attune NxT (ThermoFisher Scientific). Cell cycle was quantified using FlowJo software v10.10.0 (FlowJo LLC).

Western Blotting

Cells after treatment were lysed in radio-immunoprecipitation assay (RIPA) buffer (150 mM NaCl, 1.0% IGEPAL CA- 630, 0.5% sodium deoxycholate, 0.1% SDS, and 50 mM Tris, pH 8.0, 2 mM EDTA, 50 mM NaF) supplemented with protease inhibitor cocktail (Sigma-Aldrich

#539134-1ML) and phosphatase inhibitor cocktails 2 and 3 (Sigma-Aldrich #P5726-1ML #P0044-5ML). Protein concentrations were normalized using a Bradford protein assay (Bio-Rad #5000006). Lysates were prepared at 1 μg/μl concentration in 1X XT Sample Buffer (Bio-Rad #1610791) and 5% 2- mercaptoethanol (Sigma-Aldrich). Lysates were run on 4-12% Bolt Bis-Tris Plus gels (Life Technologies) and transferred onto nitrocellulose membranes.

The filters were blocked in 5% milk for 1h at room temperature and then incubated overnight at 4° with specific antibodies: PUMA (1:1000 Cell Signaling #12450), unprenylated RAP1A (1:50 Santa Cruz sc-373968), p44/42 MAPK (Erk1/2) (1:1000 Cell Signaling #4696), c-Myc (1:1000 Cell Signaling #18583) Vinculin (1:1000 Cell Signaling #13901), GILZ (1:1000 ThermoFisher Scientific # 12352-1-AP), Mcl1 (1:1000 Cell Signaling #39224). The following secondary HRP-conjugated antibodies were used: anti-mouse IgG, anti-rabbit IgG (1:5000 Promega #W4021 #W4011).

Chemiluminescence detected using a Nikon D700 SLR camera or the SynGene G:Box. Images were processed with auto-contrast uniformly across the entire image and densitometry was performed using ImageJ software.

Plasmid cloning, virus production and infection

CRISPR-Cas9–mediated gene knockout was generated using the lentiCRISPR v2 vector (Addgene plasmid #52961). For sgRNA cloning, the vector was linearized with BsmBI (New England Biolabs) and ligated with gene-specific sgRNAs using T4 DNA ligase (New England Biolabs). Guide RNAs targeting *BBC3* (PUMA; CGCTGGGCACGGGCGACTCC) or *TSC22D3* (GILZ; GGUGUUCUCACGCUCUAGCU) were cloned into the vector, and all constructs were confirmed by Sanger sequencing. Lentiviral particles were produced by co-transfecting 293T

HEK cells with the sgRNA containing lentiCRISPR v2 plasmid (Addgene plasmid #52961) and the packaging plasmids pCMV-VSVG (Addgene plasmid #454) and psPAX2 (Addgene plasmid #12260), using TransIT-LT1 Transfection Reagent (Mirus Bio #MIR6703) according to the manufacturer's instructions. Viral supernatant was collected 72 hours post-transfection. Target cells (1×10^5) were infected with a virus-containing supernatant and incubated at 37°C with 5% CO_2 for 5-7 days. Transduced cells were selected with puromycin at 2 μg/mL for 5–7 days, followed by 1 μg/mL for an additional 5 days, and maintained in 0.5 μg/mL thereafter. Gene knockout was confirmed by Western blotting in each experiment. Single-cell clones were generated by seeding transduced cells into 96-well plates at a density of 0.3 cells/well. Clonal populations were expanded, and those with confirmed gene knockout by western blotting were selected for downstream assays.

RNA Sequencing and Analysis

Cells were treated for 16 hours with inhibitors before being pelleted, washed, and flash frozen prior to RNA extraction. RNA was extracted using RNeasy Mini kit (QIAGEN, Germantown, MD, USA #74104) or Direct-zol RNA Microprep Kit (Thomas Scientific #1159U97) followed by on-column DNase I digestion as per manufacturer's instructions. The purity and concentration of the extracted RNA were assessed using Nanodrop before downstream applications. RNA was sent to UCI Genomic High Throughput Facility for library preparation and sequencing. In brief, library preparation was conducted using the TruSeq Stranded mRNA kit. Multiplexed samples were sequenced on the Illumina HiSeq 4000. A minimum of 40 million paired end reads were acquired for differential expression analysis and differential transcript utilization analysis. Raw fastq files generated by sequencing were quality assessed by

Fastqc/0.11.9. Transcript-level quantification was performed on a high-performance compute cluster using Salmon v1.8.0 in quasi-mapping mode and a pre-built transcriptome index obtained from the DataBio RefGenomes repository (hg38/salmon_sa_index) made from the GCA_000001405.15 GRCh38_no_alt_analysis_set from NCBI. Transcript quantification for paired-end RNA-seq libraries was performed using the –validateMappings, --seqBias, and –gcBias flags to enable selective alignment and bias correction. –useVBOpt invoked variational Bayesian optimization and –numBootstraps 30 generated 30 bootstrap replicates per sample for transcript level to gene level conversion. Outputs were imported with tximeta using countsFromAbundance= "scaledTPM" for length-scaled counts. Transcript abundances were summarized to gene level with summarizeToGene. Gene-level differential expression analysis used DESeq2 with ~ batch + condition design. Batch effects were removed with limma removeBatchEffect and matrix was rlog transformed for sample-distance heatmaps. Shrunken log2fold changes were obtained with apeglm for visualizations. Significance threshold was padj <0.05. To compare DEGs across treatments, we generated two complementary visual summaries: UpSet plots using Complex Upset package in R and scaled ellipse Venn diagrams using eulerr. We also assessed DEGs by preranked GSEA with clusterProfiler using rank= sign(log2FC)*-log10(padj) from DESeq2 output as the rank metric per treatment or the average of rank per of two treatments within a cell line. We queried Reactome via Reactome PA, and Hallmark via msigdbr. Significant GSEA results were visualized by enrichplot dot plots. These significant GSEA results were compared across groups (either treatments within a cell line or the same treatment across cell lines) in R with terms filtered at $q \leq 0.05$ in dot plots built with ggplot2 with shared terms being included and outlined along with top 20 terms per group. Heatmaps were made in pheatmap using normalized counts from DESeq2. Counts were transformed as

log2(count+1) and averaged per gene within each cell line and treatment group. For each gene, per-cell-line log2 fold changes were calculated as the difference between the mean log2 expression of each treatment and the corresponding vehicle control. To facilitate visual comparison of induction and repression patterns of significant genes across conditions in different genetic backgrounds, log2 fold changes were range-scaled within each cell line (and as such within each generalized linear model) so that the log2 fold change of gene each across all treatments is divided by the largest absolute log2 fold change for that gene in that line at the expense of absolute magnitude. These were plotted with hierarchical clustering of both genes and treatment conditions (Euclidean distance, complete linkage) to group genes by similarity in directional pattern. Absolute differences were visualized by bar plots in ggplot2 of DESeq2 apeglm shrunken log 2 fold changes and their standard errors (lfcSE).

Seahorse Assay

XF assays were performed using the Agilent Seahorse XFe96 Extracellular Flux Analyzer. The day before the assay, the sensor cartridge was placed into the calibration buffer medium supplied by Seahorse Biosciences to hydrate overnight. Seahorse XFe96 microplates wells were coated with 25 µL of Cell-Tak (Corning; Cat#354240) solution at a concentration of 22.4 µg/ml at room temperature for 20 minutes, washed twice with distilled water, and kept at 4 °C overnight. On the day of the experiment, AML cells were plated at a density of 80,000 cells per well for cell lines in XF base minimal DMEM media containing 11 mM glucose, 1 mM pyruvate and 2 mM glutamine. Then 180 µL of XF base minimal DMEM medium was added to each well and the microplate was centrifuged at 100 x g for 1 min with no break. After no more than one hour of incubation at 37 °C in CO2 free-atmosphere, basal oxygen consumption rate (OCR, as a

mitochondrial respiration indicator) and extracellular acidification rate (ECAR, as a glycolysis indicator) were performed using the Seahorse XF Cell Mito Stress Test Kit (#103015-100).

Mitochondrial Membrane Potential

Cells were treated for 16 hr with inhibitors before a subset of untreated cells wee stained with 30 μM carbonyl cyanide m-chlorophenylhydrazone (CCCP) (MedChemExpress #HY-100941) for 15 min, away from light at 37°C, 5% CO_2. Cells were then stained with 100 nM tetramethyl-rhodamine ethyl ester perchlorate (TMRE) (MedChemExpress #HY-D0985A) for 15 min, away from light at 37°C, 5% CO_2. 10,000 events were collected by an Agilent Novocyte Quanteon flow cytometer. Percent mitochondrial membrane potential loss was determined on FlowJo by sub-gating on live cells in the EYFP channel that have shifted relative to the vehicle cells.

Measurement of mitochondrial mass

Cells were treated for 16 hours with inhibitors before a subset of untreated cells are stained with 30 μM CCCP (MedChemExpress #HY-100941) for 15 minutes, away from light at 37°C, 5% CO_2. Cells were then stained for cardiolipin with 250 nM Acridine Orange 10-Nonyl Bromide (NAO) (MedChemExpress #HY-D0993) and Zombie NIR Fixable Viability kit (total dilution 1:10,000) (Biolegend #423105) for 15 minutes, away from light at 37°C, 5% CO_2. 50,000 events were collected by an Agilent Novocyte Quanteon flow cytometer. MFI was determined by first gating on live cells using the APC/Cy7 channel, then sub-gated on cells using the Pacific Orange channel. MFI was then calculated from the histogram curve.

Mitochondrial mass in viable cells was measured by flow cytometry using Tom20 Antibody (5-10) Alexa Fluor488 (Santa Cruz #17764)

Mitochondrial DNA copy number

Cells were treated for 16 hours with inhibitors before being pelleted and lysed with mouse genotyping lysis buffer and Proteinase K (ThermoFisher Scientific #EO0491). Genomic DNA was isolated using phenol-chloroform 1:1 extraction, and ethanol precipitated overnight. DNA was spun down at maximum speed for 30 minutes, washed with 70% ethanol, and re-spun at maximum speed for another 30 minutes to remove remaining ethanol. The DNA pellet was resuspended in TE buffer. Quantitative PCR was run on each condition in triplicates with genomic DNA primers for *β2M* (forward: CGACGGGAGGGTCGGGACAA; reverse: GCCCCGCGAAAGAGCGGAAG) or mitochondrial DNA primers for *ND1* (forward: GTCAACCTCGCTTCCCCACCCT; reverse: TCCTGCGAATAGGCTTCCGGCT), and PowerUp SYBR Green Master Mix (ThermoFisher Scientific #A25742). Mitochondrial DNA copy number was calculated using the following equation:

ΔC_t = *ND1* average C_t - *β2M* average C_t

Mitochondrial DNA copy number = $(1/(2^{\Delta Ct})) * 2$

Cytochrome C staining

Cells after treatment were washed in PBS and resuspended in Newmeyer Buffer. Cells were permeabilized with 0.01% digitonin for 5 min, fixed in 4% PFA for 20 min. After neutralizing PFA with neutralizing buffer (1.7M Tris Base, 1.25M Glycine, pH 9.1) samples were stained overnight with Alexa Fluor 647 Cytocrome C (#612310 Biolegend) in 10X tween intracellular staining buffer. Cytochrome c release was measured by the Novocyte 3000 or Novocyte Quanteon (Agilent) and quantified using FlowJo software v10.10.0 (FlowJo LLC).

Metabolomics

Cells were harvested and snap-frozen on dry ice. An ice-cold mixture of methanol:acetonitrile:water (40:40:20, vol; 0.5-0.6 mL) was added to samples and centrifuged at 16,000 x g for 10 min at 4°C. Supernatants (3 µL) from samples were analyzed as described (Jung et al. 2021). Briefly, a quadrupole-orbitrap mass spectrometer (Q Exactive Plus, ThermoFisher Scientific) operated in negative or positive ionization mode was coupled to a Vanquish Ultra High-Performance LC system (Thermo Fisher Scientific) with electrospray ionization. Scan range was m/z 70-1000, scanning frequency was 2 Hz and resolution was 140,000. LC separations were conducted using a XBridge BEH Amide column (2.1 mm x 150 mm2, 2.5 µm particle size, 130Å pore size pore size; Waters Corporation) with a gradient consisting of solvent A (20 mM ammonium acetate, 20 mM ammonium hydroxide in 95:5 water:acetonitrile, pH 9.45) and solvent B (acetonitrile). The flow rate was 0.150 mL/min. The gradient was: 0 min,85% B; 2 min, 85% B; 3 min, 80% B; 5 min, 80% B; 6 min, 75% B; 7 min, 75% B; 8 min, 70% B; 9 min, 70% B; 10 min, 50% B; 12 min, 50% B; 13 min, 25% B; 16 min, 25% B; 18 min, 0% B; 23 min, 0% B; 24 min, 85% B; 30 min, 85% B. Autosampler temperature was 5°C. Data were analyzed using the MAVEN software (Build # 682), Compound Discoverer software (Thermofisher Scientific), and R software. To control for instrument variability, an internal control [13C5, 15N]-valine, was spiked in the extraction solvent.

Statistics and experimental design

Statistical analysis was performed in Prism10 using one-way or two-way ANOVA, as appropriate for each experiment and indicated in the legends. Post-tests for multiple comparisons

were recommended by Prism and applied as noted in the Figure legends. All samples represent biological replicates. Unless otherwise specified in figure legends, all center values shown in graphs refer to the mean. The number of biological replicates (n) and details of the tests are provided in the figure legends. $p < 0.05$ was considered statistically significant and was annotated throughout as * $p < 0.05$, ** $p < 0.01$, *** $p < 0.001$ and **** $p < 0.001$.

No samples were excluded from analysis, and power analyses to determine sample size were not used. Studies were not conducted blinded.

Data Availability

The datasets produced in this study will be available in the following databases:

RNA-seq data: ArrayExpress (deposit is in progress).

Metabolomics data: MetaboLights (deposit is pending).

Acknowledgements

The authors thank Dr. Elizabeth Brèm and Dr. Joel Leverson for helpful discussions. We acknowledge and appreciate research contributions from undergraduate students Nilufar Montazer, Ashley Navarro, Bita Sadrossadat, Jennifer Ly, Harrison Unger, and Enoc Ulloa. This work was supported by the UC Irvine Training Program for Interdisciplinary Cancer Research (T32-CA009054, to DJ), the UPenn Hematology Clinical Research Training Program (T32-HL0439, to SJS), research grants from the National Institutes of Health (R01-AA029124 to CJ; U54CA283759, to MC), an Impact Award from the Department of Defense Peer-Reviewed Cancer Research Program (W81XWH-20-1-0867, to DAF), a Veterans Merit Award (I01BX000918, to MC), a Discovery Boost grant from the American Cancer Society (DBG-24-1319247, to DAF), a Pew Scholar Award (to CJ), the American Society of Hematology (to SJS), American Society of Clinical Oncology (to SJS), and by an Anti-Cancer Challenge pilot grant (to DAF) from the Chao Family Comprehensive Cancer Center (supported by P30-CA062203). The project utilized Shared Resources of the Chao Family Comprehensive Cancer Center (Optical Biology Core; Biostatistics Shared Resource; Experimental Tissue Resource).

Disclosure and Competing Interests Statement

SMS is co-inventor of GGTI-2418 and GGTI-2417, and is Scientific Founder of Prescient Therapeutics. MK receives research support and serves a consultant and advisory board member for AbbVie. The other authors have no competing interests to disclose.

The Paper Explained

PROBLEM: There is an unmet clinical need to overcome resistance to the BCL2 inhibitor venetoclax in acute myeloid leukemia (AML).

RESULTS: Pitavastatin is an HMG-CoA-reductase inhibitor that is used clinically to treat high cholesterol and has optimal pharmacological properties to be repurposed for oncology indications. This study shows that pitavastatin enhances venetoclax cytoxicity in AML cell lines and primary samples, including those with prevalent mechanisms of venetoclax resistance such as *TP53* mutation, MCL-1 overexpression, and elevated oxidative metabolism. The results provide detailed insight into the molecular mechanisms of action by which pitavastatin promotes apoptosis.

IMPACT: The study reveals a clinically actionable, mechanism-based strategy to overcome common features of venetoclax resistance in AML, a blood cancer with poor prognosis.

Bibliography

Abdullah MI, de Wolf E, Jawad MJ & Richardson A (2018) The poor design of clinical trials of statins in oncology may explain their failure - Lessons for drug repurposing. *Cancer Treat Rev* 69: 84–89

Advani AS, Li H, Michaelis LC, Medeiros BC, Liedtke M, List AF, O'Dwyer K, Othus M, Erba HP & Appelbaum FR (2018) Report of the relapsed/refractory cohort of SWOG S0919: A phase 2 study of idarubicin and cytarabine in combination with pravastatin for acute myelogenous leukemia (AML). *Leuk Res* 67: 17–20

Al-Zebeeby A, Vogler M, Milani M, Richards C, Alotibi A, Greaves G, Dyer MJS, Cohen GM & Varadarajan S (2019) Targeting intermediary metabolism enhances the efficacy of BH3 mimetic therapy in hematologic malignancies. *Haematologica* 104: 1016–1025

Baudino TA, Maclean KH, Brennan J, Parganas E, Yang C, Aslanian A, Lees JA, Sherr CJ, Roussel MF & Cleveland JL (2003) Myc-mediated proliferation and lymphomagenesis, but not apoptosis, are compromised by E2f1 loss. *Mol Cell* 11: 905–914

Bhatt S, Pioso MS, Olesinski EA, Yilma B, Ryan JA, Mashaka T, Leutz B, Adamia S, Zhu H, Kuang Y, *et al* (2020) Reduced mitochondrial apoptotic priming drives resistance to BH3 mimetics in acute myeloid leukemia. *Cancer Cell* 38: 872-890.e6

Bosc C, Saland E, Bousard A, Gadaud N, Sabatier M, Cognet G, Farge T, Boet E, Gotanègre M, Aroua N, *et al* (2021) Mitochondrial inhibitors circumvent adaptive resistance to venetoclax and cytarabine combination therapy in acute myeloid leukemia. *Nat Cancer* 2: 1204–1223

Bose P, Gandhi V & Konopleva M (2017) Pathways and mechanisms of venetoclax resistance. *Leuk Lymphoma* 58: 1–17

Brem EA, Shieh K, Juarez D, Buono R, Jeyakumar D, O'Brien S, Taylor TH & Fruman DA (2024) A phase 1 study of adding pitavastatin to venetoclax-based therapy in AML and CLL/SLL: a tolerable, mechanism-based, drug repurposing strategy. *Blood Neoplasia*: 100036

Brown FC, Wang X, Birkinshaw R, Chua CC, Morley T, Kasapgil S, Pomilio G, Blombery P, Huang DCS, Czabotar P, *et al* (2025) Acquired BCL2 variants associated with venetoclax resistance in acute myeloid leukemia. *Blood Adv* 9: 127–131

Caenepeel S, Brown SP, Belmontes B, Moody G, Keegan KS, Chui D, Whittington DA, Huang X, Poppe L, Cheng AC, *et al* (2018) AMG 176, a Selective MCL1 Inhibitor, Is Effective in Hematologic Cancer Models Alone and in Combination with Established Therapies. *Cancer Discov* 8: 1582–1597

Catapano AL (2010) Pitavastatin - pharmacological profile from early phase studies. *Atheroscler Suppl* 11: 3–7

Catapano AL (2012) Pitavastatin: a different pharmacological profile. *Clin Lipidol* 7: 3–9

Clendening JW & Penn LZ (2012) Targeting tumor cell metabolism with statins. *Oncogene* 31: 4967–4978

Cory S, Roberts AW, Colman PM & Adams JM (2016) Targeting BCL-2-like Proteins to Kill Cancer Cells. *Trends Cancer* 2: 443–460

Daver N, Vyas P, Huls G, Döhner H, Maury S, Novak J, Papayannidis C, Martínez Chamorro C, Montesinos P, Niroula R, *et al* (2025) The ENHANCE-3 study: venetoclax and azacitidine plus magrolimab or placebo for untreated AML unfit for intensive therapy. *Blood* 146: 601–611

Davids MS, Brander DM, Alvarado-Valero Y, Diefenbach CS, Egan DN, Dinner SN, Javidi-Sharifi N, Al Malki MM, Begna KH, Bhatt VR, *et al* (2025) A phase 1 study of the CDK9

inhibitor voruciclib in relapsed/refractory acute myeloid leukemia and B-cell malignancies. *Blood Adv* 9: 820–832

Desai P, Lonial S, Cashen A, Kamdar M, Flinn I, O'Brien S, Garcia JS, Korde N, Moslehi J, Wey M, *et al* (2024) A Phase 1 First-in-Human Study of the MCL-1 Inhibitor AZD5991 in Patients with Relapsed/Refractory Hematologic Malignancies. *Clin Cancer Res* 30: 4844–4855

DiNardo CD, Jonas BA, Pullarkat V, Thirman MJ, Garcia JS, Wei AH, Konopleva M, Döhner H, Letai A, Fenaux P, *et al* (2020a) Azacitidine and venetoclax in previously untreated acute myeloid leukemia. *N Engl J Med* 383: 617–629

DiNardo CD, Pratz K, Pullarkat V, Jonas BA, Arellano M, Becker PS, Frankfurt O, Konopleva M, Wei AH, Kantarjian HM, *et al* (2019) Venetoclax combined with decitabine or azacitidine in treatment-naive, elderly patients with acute myeloid leukemia. *Blood* 133: 7–17

DiNardo CD, Tiong IS, Quaglieri A, MacRaild S, Loghavi S, Brown FC, Thijssen R, Pomilio G, Ivey A, Salmon JM, *et al* (2020b) Molecular patterns of response and treatment failure after frontline venetoclax combinations in older patients with AML. *Blood* 135: 791–803

Döhner H, Pratz KW, DiNardo CD, Wei AH, Jonas BA, Pullarkat VA, Thirman MJ, Récher C, Schuh AC, Babu S, *et al* (2024) Genetic risk stratification and outcomes among treatment-naive patients with AML treated with venetoclax and azacitidine. *Blood* 144: 2211–2222

Gimenez N, Tripathi R, Giró A, Rosich L, López-Guerra M, López-Oreja I, Playa-Albinyana H, Arenas F, Mas JM, Pérez-Galán P, *et al* (2020) Systems biology drug screening identifies statins as enhancers of current therapies in chronic lymphocytic leukemia. *Sci Rep* 10: 22153

Glytsou C, Chen X, Zacharioudakis E, Al-Santli W, Zhou H, Nadorp B, Lee S, Lasry A, Sun Z, Papaioannou D, *et al* (2023) Mitophagy promotes resistance to BH3 mimetics in acute myeloid leukemia. *Cancer Discov* 13: 1656–1677

Grant S (2017) Rational combination strategies to enhance venetoclax activity and overcome resistance in hematologic malignancies. *Leuk Lymphoma* 59: 1–8

Grenier A, Poulain L, Mondesir J, Jacquel A, Bosc C, Stuani L, Mouche S, Larrue C, Sahal A, Birsen R, *et al* (2022) AMPK-PERK axis represses oxidative metabolism and enhances apoptotic priming of mitochondria in acute myeloid leukemia. *Cell Rep* 38: 110197

Grinspoon SK, Fitch KV, Zanni MV, Fichtenbaum CJ, Umbleja T, Aberg JA, Overton ET, Malvestutto CD, Bloomfield GS, Currier JS, *et al* (2023) Pitavastatin to prevent cardiovascular disease in HIV infection. *N Engl J Med* 389: 687–699

Han L, Zhang Q, Dail M, Shi C, Cavazos A, Ruvolo VR, Zhao Y, Kim E, Rahmani M, Mak DH, *et al* (2020) Concomitant targeting of BCL2 with venetoclax and MAPK signaling with cobimetinib in acute myeloid leukemia models. *Haematologica* 105: 697–707

Hillis AL, Martin TD, Manchester HE, Högström J, Zhang N, Lecky E, Kozlova N, Lee J, Persky NS, Root DE, *et al* (2024) Targeting Cholesterol Biosynthesis with Statins Synergizes with AKT Inhibitors in Triple-Negative Breast Cancer. *Cancer Res* 84: 3250–3266

Hua L, Yang N, Li Y, Huang K, Jiang X, Liu F, Yu Z, Chen J, Lai J, Du J, *et al* (2023) Metformin sensitizes AML cells to venetoclax through endoplasmic reticulum stress-CHOP pathway. *Br J Haematol* 202: 971–984

Juarez D, Buono R, Matulis SM, Gupta VA, Duong M, Yudiono J, Paul M, Mallya S, Diep G, Hsin P, *et al* (2023) Statin-induced Mitochondrial Priming Sensitizes Multiple Myeloma Cells to BCL2 and MCL-1 Inhibitors. *Cancer Res Commun* 3: 2497–2509

Juarez D & Fruman DA (2021) Targeting the mevalonate pathway in cancer. *Trends Cancer* 7: 525–540

Kervoëlen C, Ménoret E, Gomez-Bougie P, Bataille R, Godon C, Marionneau-Lambot S, Moreau P, Pellat-Deceunynck C & Amiot M (2015) Dexamethasone-induced cell death is restricted to specific molecular subgroups of multiple myeloma. *Oncotarget* 6: 26922–26934

Kornblau SM, Banker DE, Stirewalt D, Shen D, Lemker E, Verstovsek S, Estrov Z, Faderl S, Cortes J, Beran M, *et al* (2007) Blockade of adaptive defensive changes in cholesterol uptake and synthesis in AML by the addition of pravastatin to idarubicin + high-dose Ara-C: a phase 1 study. *Blood* 109: 2999–3006

Lee JS, Roberts A, Juarez D, Vo T-TT, Bhatt S, Herzog L-O, Mallya S, Bellin RJ, Agarwal SK, Salem AH, *et al* (2018) Statins enhance efficacy of venetoclax in blood cancers. *Sci Transl Med* 10(445)

Leverson JD, Sampath D, Souers AJ, Rosenberg SH, Fairbrother WJ, Amiot M, Konopleva M & Letai A (2017) Found in Translation: How Preclinical Research Is Guiding the Clinical Development of the BCL2-Selective Inhibitor Venetoclax. *Cancer Discov* 7: 1376–1393

Liu F, Kalpage HA, Wang D, Edwards H, Hüttemann M, Ma J, Su Y, Carter J, Li X, Polin L, *et al* (2020) Cotargeting of Mitochondrial Complex I and Bcl-2 Shows Antileukemic Activity against Acute Myeloid Leukemia Cells Reliant on Oxidative Phosphorylation. *Cancers (Basel)* 12

Longo J, van Leeuwen JE, Elbaz M, Branchard E & Penn LZ (2020) Statins as anticancer agents in the era of precision medicine. *Clin Cancer Res* 26: 5791–5800

Luo Z, Zhang Y, Gu J, Feng P & Wang Y (2015) Pharmacokinetic Properties of Single- and Multiple-Dose Pitavastatin Calcium Tablets in Healthy Chinese Volunteers. *Curr Ther Res Clin Exp* 77: 52–57

Merino D, Kelly GL, Lessene G, Wei AH, Roberts AW & Strasser A (2018) BH3-Mimetic Drugs: Blazing the Trail for New Cancer Medicines. *Cancer Cell* 34: 879–891

Molina JR, Sun Y, Protopopova M, Gera S, Bandi M, Bristow C, McAfoos T, Morlacchi P, Ackroyd J, Agip A-NA, *et al* (2018) An inhibitor of oxidative phosphorylation exploits cancer vulnerability. *Nat Med* 24: 1036–1046

Moujalled DM, Pomilio G, Ghiurau C, Ivey A, Salmon J, Rijal S, Macraild S, Zhang L, Teh T-C, Tiong I-S, *et al* (2019) Combining BH3-mimetics to target both BCL-2 and MCL1 has potent activity in pre-clinical models of acute myeloid leukemia. *Leukemia* 33: 905–917

Mullen PJ, Yu R, Longo J, Archer MC & Penn LZ (2016) The interplay between cell signalling and the mevalonate pathway in cancer. *Nat Rev Cancer* 16: 718–731

Nechiporuk T, Kurtz SE, Nikolova O, Liu T, Jones CL, D'Alessandro A, Culp-Hill R, d'Almeida A, Joshi SK, Rosenberg M, *et al* (2019) The TP53 apoptotic network is a primary mediator of resistance to BCL2 inhibition in AML cells. *Cancer Discov* 9: 910–925

Newman A, Clutterbuck RD, Powles RL & Millar JL (1994) Selective inhibition of primary acute myeloid leukaemia cell growth by simvastatin. *Leukemia* 8: 2023–2029

Pandyra A, Mullen PJ, Kalkat M, Yu R, Pong JT, Li Z, Trudel S, Lang KS, Minden MD, Schimmer AD, *et al* (2014) Immediate utility of two approved agents to target both the metabolic mevalonate pathway and its restorative feedback loop. *Cancer Res* 74: 4772–4782

Peng H, Carrico D, Thai V, Blaskovich M, Bucher C, Pusateri EE, Sebti SM & Hamilton AD (2006) Synthesis and evaluation of potent, highly-selective, 3-aryl-piperazinone inhibitors of protein geranylgeranyltransferase-I. *Org Biomol Chem* 4: 1768–1784

Pollyea DA, Pratz KW, Wei AH, Pullarkat V, Jonas BA, Recher C, Babu S, Schuh AC, Dail M, Sun Y, *et al* (2022) Outcomes in Patients with Poor-Risk Cytogenetics with or without TP53 Mutations Treated with Venetoclax and Azacitidine. *Clin Cancer Res* 28: 5272–5279

Roberts AW, Davids MS, Pagel JM, Kahl BS, Puvvada SD, Gerecitano JF, Kipps TJ, Anderson MA, Brown JR, Gressick L, *et al* (2016) Targeting BCL2 with Venetoclax in Relapsed Chronic Lymphocytic Leukemia. *N Engl J Med* 374: 311–322

Sango J, Carcamo S, Sirenko M, Maiti A, Mansour H, Ulukaya G, Tomalin LE, Cruz-Rodriguez N, Wang T, Olszewska M, *et al* (2024) RAS-mutant leukaemia stem cells drive clinical resistance to venetoclax. *Nature* 636: 241–250

Schonewille M, de Boer JF, Mele L, Wolters H, Bloks VW, Wolters JC, Kuivenhoven JA, Tietge UJF, Brufau G & Groen AK (2016) Statins increase hepatic cholesterol synthesis and stimulate fecal cholesterol elimination in mice. *J Lipid Res* 57: 1455–1464

Schuldiner O & Benvenisty N (2001) A DNA microarray screen for genes involved in c-MYC and N-MYC oncogenesis in human tumors. *Oncogene* 20: 4984–4994

Sharon D, Cathelin S, Mirali S, Di Trani JM, Yanofsky DJ, Keon KA, Rubinstein JL, Schimmer AD, Ketela T & Chan SM (2019) Inhibition of mitochondrial translation overcomes venetoclax resistance in AML through activation of the integrated stress response. *Sci Transl Med* 11(516)

Skuli SJ, Bakayoko A, Kruidenier M, Manning B, Pammer P, Salimov A, Riley O, Brake-Sillá G, Dopkin D, Bowman M, *et al* (2025) Chemoresistance of TP53 mutant acute myeloid leukemia requires the mevalonate byproduct, geranylgeranyl pyrophosphate, for induction of an adaptive stress response. *Leukemia* 39: 2087–2098

Teh TC, Nguyen N-Y, Moujalled DM, Segal D, Pomilio G, Rijal S, Jabbour A, Cummins K, Lackovic K, Blombery P, *et al* (2017) Enhancing venetoclax activity in acute myeloid leukemia by co-targeting MCL1. *Leukemia* 32: 303–312

Thijssen R, Diepstraten ST, Moujalled D, Chew E, Flensburg C, Shi MX, Dengler MA, Litalien V, MacRaild S, Chen M, *et al* (2021) Intact TP-53 function is essential for sustaining durable responses to BH3-mimetic drugs in leukemias. *Blood* 137: 2721–2735

Tripathi S, Gupta E & Galande S (2024) Statins as anti-tumor agents: A paradigm for repurposed drugs. *Cancer Rep* 7: e2078

Valentin R, Grabow S & Davids MS (2018) The rise of apoptosis: targeting apoptosis in hematologic malignancies. *Blood* 132: 1248–1264

Velez J, Pan R, Lee JTC, Enciso L, Suarez M, Duque JE, Jaramillo D, Lopez C, Morales L, Bornmann W, *et al* (2016) Biguanides sensitize leukemia cells to ABT-737-induced apoptosis by inhibiting mitochondrial electron transport. *Oncotarget* 7: 51435–51449

Wang M & Casey PJ (2016) Protein prenylation: unique fats make their mark on biology. *Nat Rev Mol Cell Biol* 17: 110–122

Wong WW-L, Clendening JW, Martirosyan A, Boutros PC, Bros C, Khosravi F, Jurisica I, Stewart AK, Bergsagel PL & Penn LZ (2007) Determinants of sensitivity to lovastatin-induced apoptosis in multiple myeloma. *Mol Cancer Ther* 6: 1886–1897

Xia Y, Xie Y, Yu Z, Xiao H, Jiang G, Zhou X, Yang Y, Li X, Zhao M, Li L, *et al* (2018) The mevalonate pathway is a druggable target for vaccine adjuvant discovery. *Cell* 175: 1059-1073.e21

Xia Z, Tan MM, Wong WW, Dimitroulakos J, Minden MD & Penn LZ (2001) Blocking protein geranylgeranylation is essential for lovastatin-induced apoptosis of human acute myeloid leukemia cells. *Leukemia* 15: 1398–1407

Yap TA, Daver N, Mahendra M, Zhang J, Kamiya-Matsuoka C, Meric-Bernstam F, Kantarjian HM, Ravandi F, Collins ME, Francesco MED, *et al* (2023) Complex I inhibitor of oxidative phosphorylation in advanced solid tumors and acute myeloid leukemia: phase I trials. *Nat Med* 29: 115–126

Zeidner JF, Sallman DA, Récher C, Daver NG, Leung AYH, Hiwase DK, Subklewe M, Pabst T, Montesinos P, Larson RA, *et al* (2025) Magrolimab plus azacitidine vs physician's choice for untreated TP53-mutated acute myeloid leukemia: the ENHANCE-2 study. *Blood* 146: 590–600

Zhang Q, Riley-Gillis B, Han L, Jia Y, Lodi A, Zhang H, Ganesan S, Pan R, Konoplev SN, Sweeney SR, *et al* (2022) Activation of RAS/MAPK pathway confers MCL-1 mediated acquired resistance to BCL-2 inhibitor venetoclax in acute myeloid leukemia. *Signal Transduct Target Ther* 7: 51

Figure Legends

Figure 1: Pitavastatin has potent cytotoxicity in venetoclax-resistant AML cell lines and in patient-derived AML cells. (A) AML cell lines were treated for 48hr with various concentrations of venetoclax alone or with pitavastatin (PIT) at 0.3, 1 and 3 μM. Data are expressed as mean +/- SEM *$p < 0.05$, ****$p < 0.0001$. Two-way ANOVA with Tukey's post hoc test. (B) Patient-derived AML myeloblasts cultured in media with supportive cytokines were treated for 48hr with titrated concentrations of PIT and venetoclax as indicated. For both panels the percentage of viable cells was determined by flow cytometry using Annexin V and PI staining. Identified genetic lesions are shown in parentheses – note three *TP53* mutant samples on the bottom row were all pitavastatin-sensitive.

Figure 2: PUMA upregulation contributes to pitavastatin cytotoxicity, is dependent on GGPP depletion, and is recapitulated by inhibition of GGTase-1. (A) The cytotoxic effect of pitavastatin +/- 30nM venetoclax was measured in two clones of OCI-AML3 cells with PUMA knockout and one clone each of MOLM14 and MOLM13. Two-way ANOVA with Tukey's post hoc test, $n = 3$. (B) PUMA expression in a statin-sensitive AML cell line (OCI-AML3) was assessed by western blot. An antibody to vinculin was used as a loading control. Detection of unprenylated RAP1A was used to determine which treatments suppress protein geranylgeranylation. Note rescue of PIT effect on PUMA by mevalonate (MEV) and GGPP more than by FPP. (C) Quantitation of four replicates of the experiment in panel B, with PUMA expression in vehicle (Veh) treated cells set at 1. Data are expressed as mean +/- SEM ** $p < 0.01$, ***$p < 0.001$, one-way ANOVA with Tukey's post hoc test, $n = 2$-4. (D-E) Different GGTase-1 inhibitors have distinct effects on PUMA expression and viability. (D) Representative

western blot of PUMA expression in OCI-AML3 and MOLM13 treated with pitavastatin (0.3 or 1 μM), GGTI298 (10 μM) or GGTI2133 (10 μM).

(E) Graphs showing percentage of viable OCI-AML3 and MOLM13 measured by Annexin V and PI staining after 48h of treatment with pitavastatin (1 μM+, GGTI298 (10 μM) or GGTI2133 (10 μM) in combination with venetoclax. Data are expressed as mean +/- SEM ***$p < 0.001$, ****$p < 0.0001$. Two-way ANOVA with Tukey's post hoc test, $n \geq 3$.

Figure 3: Transcriptome analysis identifies shared features of the response to PIT and GGTI-298. (A) DEGs in OCI-AML3 cells treated with PIT, GGTI-298, or GGTI-2133, relative to vehicle, were identified by DESeq2, and DEG overlaps were depicted by Venn diagrams and summarized with UpSet plots. (B) GSEA for hallmark and reactome pathways shared by treatment with PIT or GGTI-298. Red indicates GSEA pathways that are upregulated, blue downregulated. Outlined dots are pathways shared in both OCI-AML3 and HNT-34, including downregulation of MYC and E2F targets, and aerobic respiration. The diameter of each dot corresponds to gene set size.

Figure 4: Transcriptome analysis identifies features of the response to PIT that depend on GGPP depletion. (A) Venn diagram and intersection plot showing DEGs in OCI-AML3 cells treated with PIT, GGPP, or PIT + GGPP, compared to vehicle. Note that in the presence of exogenous GGPP, PIT treatment induced very few gene expression changes. (B) GSEA for hallmark (left, including MYC and E2F targets) and reactome pathways (right, including mitochondrial protein import). The p value decreases from blue to red colors, and the diameter of each dot corresponds to gene set size.

Figure 5: Pitavastatin treatment downregulates cMYC expression and increases PUMA and GILZ in AML cell lines and primary cells. (A) Two PIT-sensitive cell lines, one PIT-resistant cell line, and two PIT-sensitive primary AML samples were treated for 16hr as indicated and lysates subjected to western blotting with antibodies to cMYC, PUMA, GILZ, unprenylated RAP1A, and total ERK. (B) Graph of quantitation of western blots from 3-4 experiments for cell lines in panel A, or single experiment for two primary cell samples UCI-01 and UCI-06. Data are expressed as mean +/- SEM *$p < 0.05$, ***$p < 0.001$, ****$p < 0.0001$ two-way ANOVA with Dunnett's test. (C) PIT and GGTI-298 cause G1 arrest in OCI-AML3 cells that are statin sensitive and show consistent MYC downregulation, but not in HNT-34 cells where MYC downregulation is less prominent. Data are expressed as mean +/- SEM *$p < 0.05$, ** $p < 0.01$, ****$p < 0.0001$ two-way ANOVA with Tukey's test, n = 3.

Figure 6: Functional assays provide evidence that PIT causes mitochondrial dysfunction. (A) Heat map of nuclear-encoded mitochondrial genes (MitoCarta database) across conditions in both transcriptome experiments. (B-D) Oxygen consumption rate (OCR) was measured by Seahorse metabolic flux analyzer. (B) Representative Seahorse assay traces in OCI-AML3 and MOLM13 cells treated with vehicle or pitavastatin for 16hr. (C) Graphs depict results of experiments as in panel B, shown as mean +/- SEM, **** $p < 0.0001$ two-way ANOVA with Sidak's test, n = 8. (D) Effect of pitavastatin on basal OCR is significantly reversed by GGPP. * $p < 0.05$, **** $p < 0.0001$ two-way ANOVA with Fisher's least squares difference test, n = 5. (E) ^{13}C-glucose tracing identifies reduced TCA cycle intermediates in OCI-AML3 cells treated with pitavastatin for 16hr (13C-glucose added for last 2hr). Left graph shows quantitation of

glycolytic metabolites, lactate, and acetyl-CoA, containing all ^{13}C atoms traced. Right graph shows TCA cycle metabolites with ^{13}C in M+2 position. Each dot plot depicts results of 3 biological replicates, each representing 4-6 technical replicates, normalized as a ratio of the pitavastatin-treated sample to the vehicle-treated group. * $p < 0.05$, ** $p < 0.01$, *** $p < 0.001$ two-way ANOVA with Fisher's least squares difference test (^ $p = 0.051$ for lactate as marked).

Expanded View Figure Legends

Figure EV1: (A) Pitavastatin has cytotoxic activity at 24hr that is prevented by caspase inhibitor QVD-OPH. (B) PIT retains cytotoxic activity in VEN-resistant MOLM13-R cells. (C) Simvastatin is less potent in AML cell lines, with effective concentratons of 3 or 10 μM. Data are expressed as mean +/- SEM *$p < 0.05$, ** $p < 0.01$, ***$p < 0.001$, ****$p < 0.0001$ two-way ANOVA, n = 3.

Figure EV2: (A, B) Additional viability assays on primary samples treated with pitavastatin alone (A) or in combination with venetoclax (B). (C) PIT increases cytotoxicity of VEN-AZA (5Aza) combo in primary AML samples. Data are expressed as mean +/- SEM. Genetic lesions are shown in parentheses.

Figure EV3: PIT cytotoxicity and VEN sensitization is preserved in isogenic MOLM14 cell lines with *TP53* mutation. Graphs showing percentage of Annexin V and PI negative cells after treatment with different concentrations of pitavastatin in combination with venetoclax. Data are expressed as mean +/- SEM *$p < 0.05$, ** $p < 0.01$, ***$p < 0.001$, ****$p < 0.0001$. Two-way ANOVA with Tukey post hoc test, $n \geq 3$.

Figure EV4: PUMA upregulation in additional statin-sensitive and resistant cell lines. (A-B) Western blots were used to measure PUMA expression in pitavastatin sensitive (OCI-AML3, HNT-34) and insensitive (OCI-M1) AML cell lines. The PL-21 cell line is designated "weakly sensitive" because PIT alone has no cytotoxic effect but slightly enhances venetoclax cytotoxicity. Relative protein quantification performed by densitometric analysis using ImageJ64

software. Data are expressed as mean +/- SEM *p < 0.05, ** p < 0.01, ***p < 0.001, ****p < 0.0001. Two-way ANOVA, n ≥ 3. Similar experiments were performed to measure PUMA expression in an additional pitavastatin sensitive cell line, MV4-11 (C) and in MOLM13 where pitavastatin alone has no cytotoxic effect but sensitizes to venetoclax (D). Data are expressed as mean +/- SEM *p < 0.05, ** p < 0.01. One way ANOVA, n ≥ 3.

Figure EV5: (A) Western blots were used to measure PUMA expression in control and *TP53* mutant MOLM14 isogenic cell lines. Data are expressed as mean +/- SEM *p < 0.05, ** p < 0.01, two-way ANOVA, n = 3. (B) Western blot validation of reduced or absent PUMA expression in OCI-AML3, MOLM13 and MOLM14 cells in which the *BBC3* gene was disrupted by CRISPR. Cells were treated with vehicle or pitavastatin (1 μM) for 16hr.

Figure EV6: Pitavastatin treatment reduces or prevents the increase of MCL-1 protein expression in combination with venetoclax treatment. (A) Representative western blot of MCL-1 and PUMA protein expression in OCI-AML3, MOLM13, and MOLM14 cells following 24-hour treatments with Veh (0.1% DMSO), PIT, VEN and their combination. An antibody to vinculin was used as a loading control. (B) Quantification of relative MCL-1 and PUMA protein expression following treatment. Data are expressed as mean +/- SEM *p < 0.05, ** p < 0.01, ***p < 0.001, ****p < 0.0001 two-way ANOVA, n = 3. (C, D) PUMA and MCL1 protein analysis in MOLM13 parental and venetoclax resistant cell lines (C) and in three primary p53 mutant patient samples (D).

Figure EV7: Data supporting pitavastatin mechanism is dependent on GGPP depletion. (A) GGPP rescue of cytotoxicity in sensitive lines (OCI-AML3, HNT-34). Data are expressed as mean +/- SEM, ** $p < 0.01$, ****$p < 0.0001$ two-way ANOVA (n = 2-4). (B) PUMA expression and relative quantification in OCI-AML3 after treatment with PIT, GGTI-298 or GGPS inhibitor (THZ145). Data are expressed as mean +/- SEM *$p < 0.05$, ** $p < 0.01$, one-way ANOVA, $n \geq 3$. (C) Graphs showing percentage of viable OCI-AML3 after 48h of treatment with pitavastatin 1 μM, GGTI-298, GGTI-2133 or THZ145 in combination with venetoclax. Data are expressed as mean +/- SEM **** $p < 0.0001$, two-way ANOVA, n =3.

Figure EV8: GGTIs inhibit prenylation. (A) F-actin polymeration measured by phalloidin staining is inhibited by both GGTI-298 and GGTI-2133. Latrunculin was used as a positive control to completely disrupt actin polymerization. (B, C) All three GGTIs cause RAP1A unprenylation; GGTI-2417 increases PUMA to a similar or greater extent as GGTI-298. (D) percentage of viable OCI-AML3 treated with pitavastatin, GGTI-298 or GGTI-2417 in combination with venetoclax. Data are expressed as mean +/- SEM *$p < 0.05$, ** $p < 0.01$, ****$p < 0.0001$. Two-way ANOVA, n = 4.

Figure EV9: (A) Venn diagram and intersection plots for HNT-34 cells, similar to Figure 3A for OCI-AML3 cells. (B) PCA plots for transcriptome experiment #1. (C) Intersection plots of sample distance for OCI-AML3 (left) and HNT-34 (right). (D) Additional evidence for MYC/E2F downregulation using Ingenuity Pathway Analysis.

Figure EV10: Fold change in mRNA expression of genes of interest described in the Results section. (A) OCI-AML3 cells. (B) HNT-34 cells. (C) OCI-AML3 cells from experiment #2.

Figure EV11: (A) PCA analysis of OCI-AML3 cells analyzed in transcriptome experiment #2. (B) Venn diagram and intersection plot for MOLM13 cells in experiment #2. Consistent with minimal pitavastatin sensitivity, these cells had few DEGs. (C) GSEA analysis of data from MOLM13 cells identified cholesterol and lipid pathways as predominant gene sets.

Figure EV12: MYC downregulation in OCI-AML3 cells is recapitulated by GGTI-298 and GGTI-2417, weakly by GGTI-2133. (A) Representative western blot. (B) Relative protein quantifications. Data are expressed as mean +/- SEM *$p < 0.05$, ** $p < 0.01$, *** $p < 0.001$ one-way ANOVA, n = 3.

Figure EV13: CRISPR KO of the *TSC22D3* gene encoding GILZ does not alter PIT cytotoxicity or combo effect with VEN. (A) GILZ upregulation and MYC downregulation are rescued by GGPP. Top: representative Western blot. MM1S cells are a dexamethasone (Dex)-sensitive MM cell line used as a positive control for GILZ induction. Bottom: graphs depict quantitation of 3 experiments. Data are expressed as mean +/- SEM *$p < 0.05$, ** $p < 0.01$, **** $p < 0.0001$ two-way ANOVA. (B) Western blot showing loss of GILZ expression in knockout clones. (C) Viability assay in parental, empty vector (EV) control, and three knockout clones.

Figure EV14: Mitochondrial mass was measured in AML cell lines treated with vehicle or pitavastatin for 16hr. (A) TOM20 measured by intracellular staining and flow cytometry. (B) Mitochondrial DNA copy number relative to genomic DNA was determined by qPCR. (C)

Cardiolipin measured by intracellular staining and flow cytometry. Data are expressed as mean +/- SEM *p < 0.05, ***p < 0.001 two-way ANOVA.

Figure EV15: (A-B) Graphs showing reduction of maximal OCR and spare respiratory capacity by the combination of PIT + VEN in OCI-AML3 and MOLM13. Data are expressed as mean +/- SEM *p < 0.05, ** p < 0.01, ***p < 0.001, **** p < 0.0001 two-way ANOVA. (C, D) Flow cytometry was used to measure the percentage of cells that release Cytochrome c (Cyt-c) after 16hr of treatment. (C) In OCI-AML3 and MOLM13 cells, venetoclax alone causes Cyt-c release that is enhanced by PIT in a GGPP-dependent manner. (D) PIT + VEN causes Cyt-c release in control and *TP53* mutant MOLM14 cells. Data are expressed as mean of cytochrome-C-high cells, +/- SEM, *p < 0.05, ** p < 0.01, ****p < 0.0001 two-way ANOVA, n = 3.

Figure EV16: Pitavastatin causes loss of mitochondrial membrane potential (MMP) in a significant fraction of OCI-AML3 (A) and MOLM14 cells including *TP53*-mutant (B). MMP loss was measured by flow cytometry using TMRE staining and expressed as percent MMP-low. Data are expressed as mean +/- SEM. *p < 0.05, ** p < 0.01, by two-way ANOVA, n = 5.

Supplementary Table EV1: Characteristics of AML cell lines used in this study.

Supplementary Table EV2: Synergy scores for cell lines treated with pitavastatin/venetoclax combinations.

Supplementary Table EV3: Characteristics of primary samples used in this study.

Supplementary Table EV4: Synergy scores for MOLM14 and derivative cell lines treated with pitavastatin/venetoclax combinations.

Supplementary Data Files:

Excel File #1: DEGs lists and volcano plots for transcriptome experiment #1.

Excel File #2: DEGs lists and volcano plots for transcriptome experiment #2.

DEG lists were generated using an adjusted p value threshold of 0.05 and a $\log_2$ fold-change (LFC) threshold of +/- 0.1. Volcano plots display DEGs with a more stringent LFC threshold for ease of visualization of named genes.

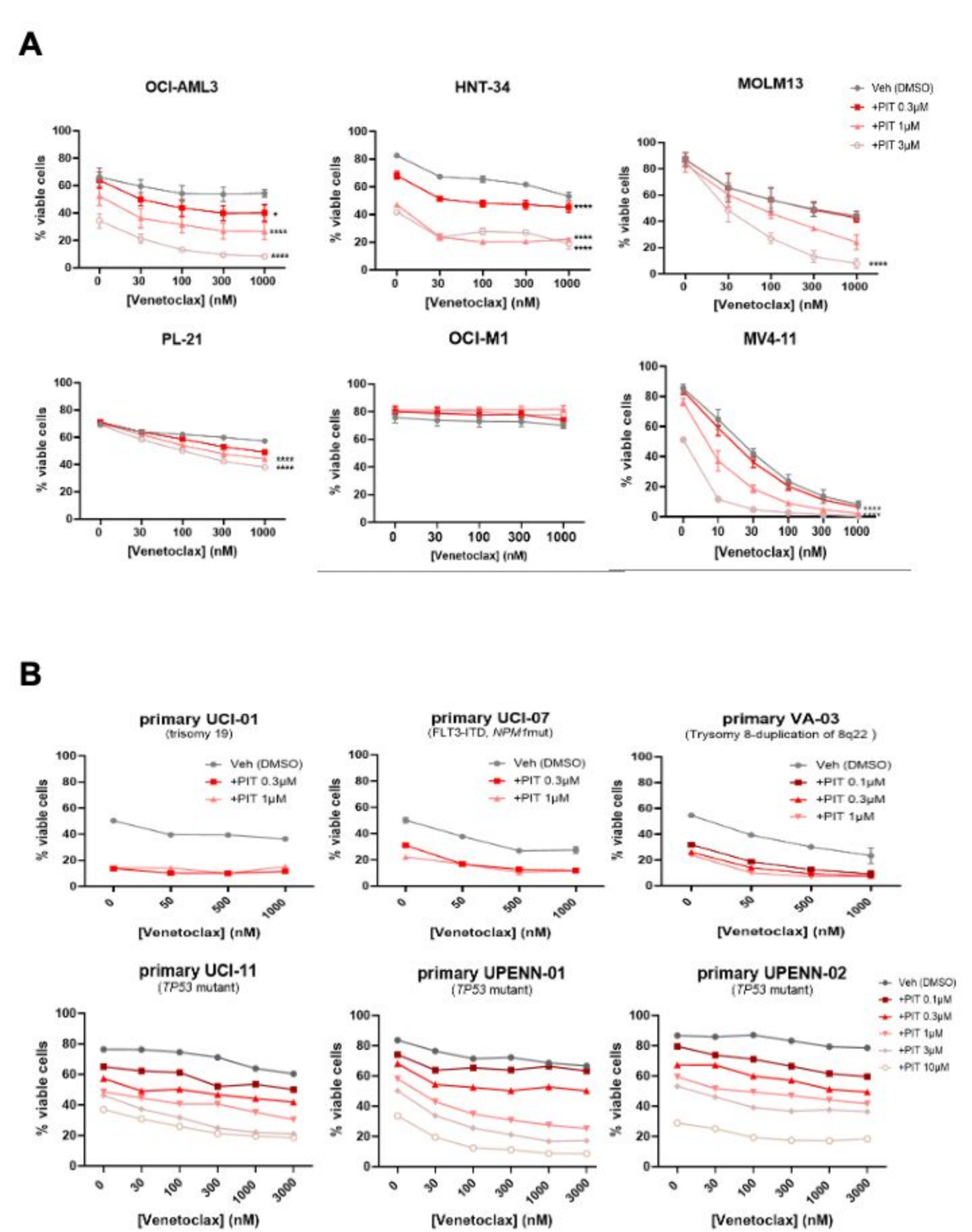
A
OCI-AML3
HNT-34
MOLM13
PL-21
OCI-M1
MV4-11
Veh (DMSO)
+PIT 0.3μM
+PIT 1μM
+PIT 3μM
% viable cells
[Venetoclax] (nM)
B
primary UCI-01
(trisomy 19)
primary UCI-07
(FLT3-ITD, NPM1mut)
primary VA-03
(Trysomy 8-duplication of 8q22)
primary UCI-11
(TP53 mutant)
primary UPENN-01
(TP53 mutant)
primary UPENN-02
(TP53 mutant)
+PIT 0.1μM
+PIT 10μM

Figure 1

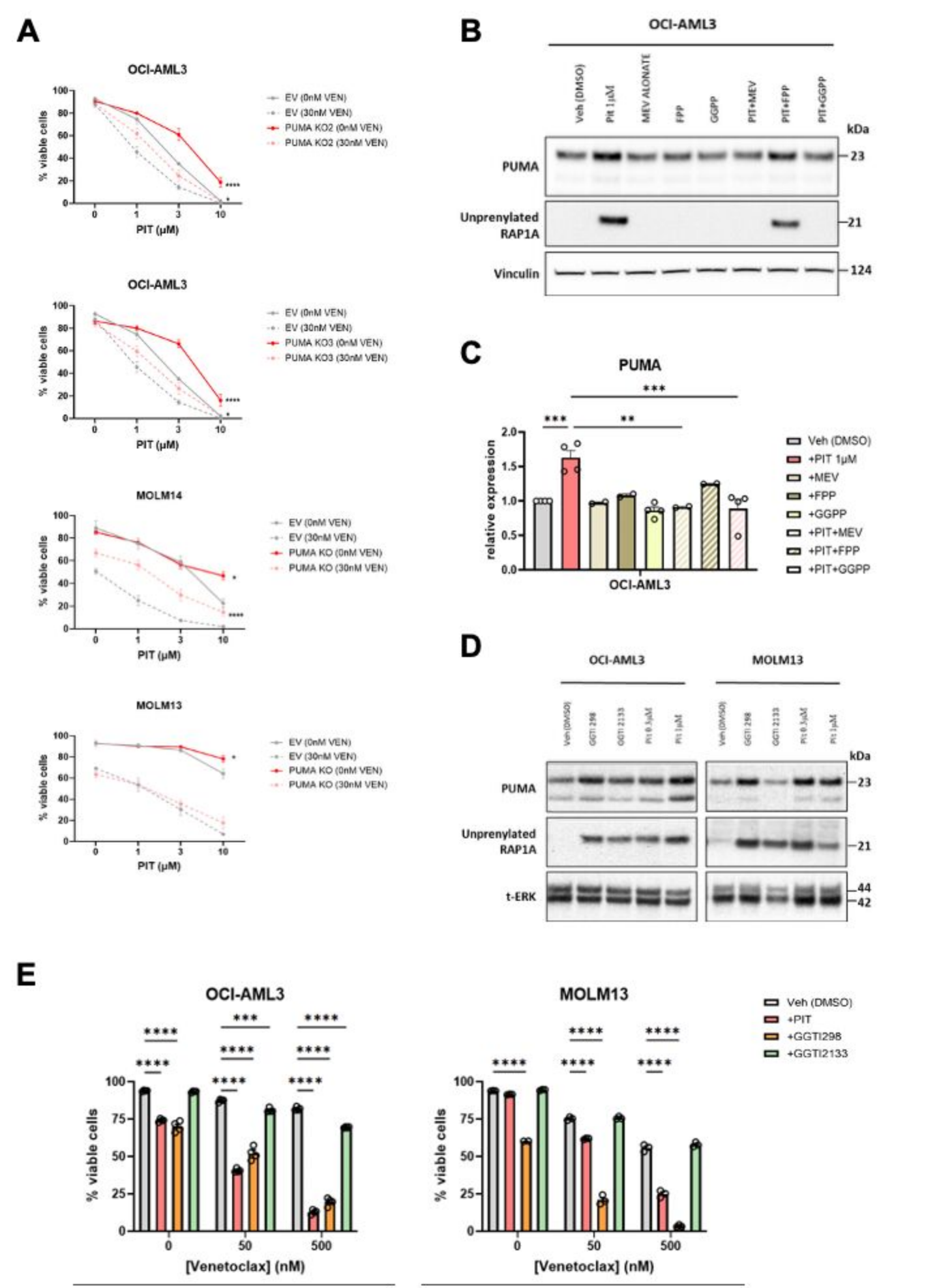
A
OCI-AML3
% viable cells
PIT (μM)
EV (0nM VEN)
EV (30nM VEN)
PUMA KO2 (0nM VEN)
PUMA KO2 (30nM VEN)
OCI-AML3
PUMA KO3 (0nM VEN)
PUMA KO3 (30nM VEN)
MOLM14
PUMA KO (0nM VEN)
PUMA KO (30nM VEN)
MOLM13
B
OCI-AML3
Veh (DMSO)
Pit 1μM
MEV ALONATE
FPP
GGPP
PIT+MEV
PIT+FPP
PIT+GGPP
kDa
PUMA
Unprenylated RAP1A
Vinculin
23
21
124
C
PUMA
relative expression
OCI-AML3
Veh (DMSO)
+PIT 1μM
+MEV
+FPP
+GGPP
+PIT+MEV
+PIT+FPP
+PIT+GGPP
D
OCI-AML3
MOLM13
PUMA
Unprenylated RAP1A
t-ERK
44
42
E
OCI-AML3
MOLM13
% viable cells
[Venetoclax] (nM)
Veh (DMSO)
+PIT
+GGTI298
+GGTI2133

Figure 2

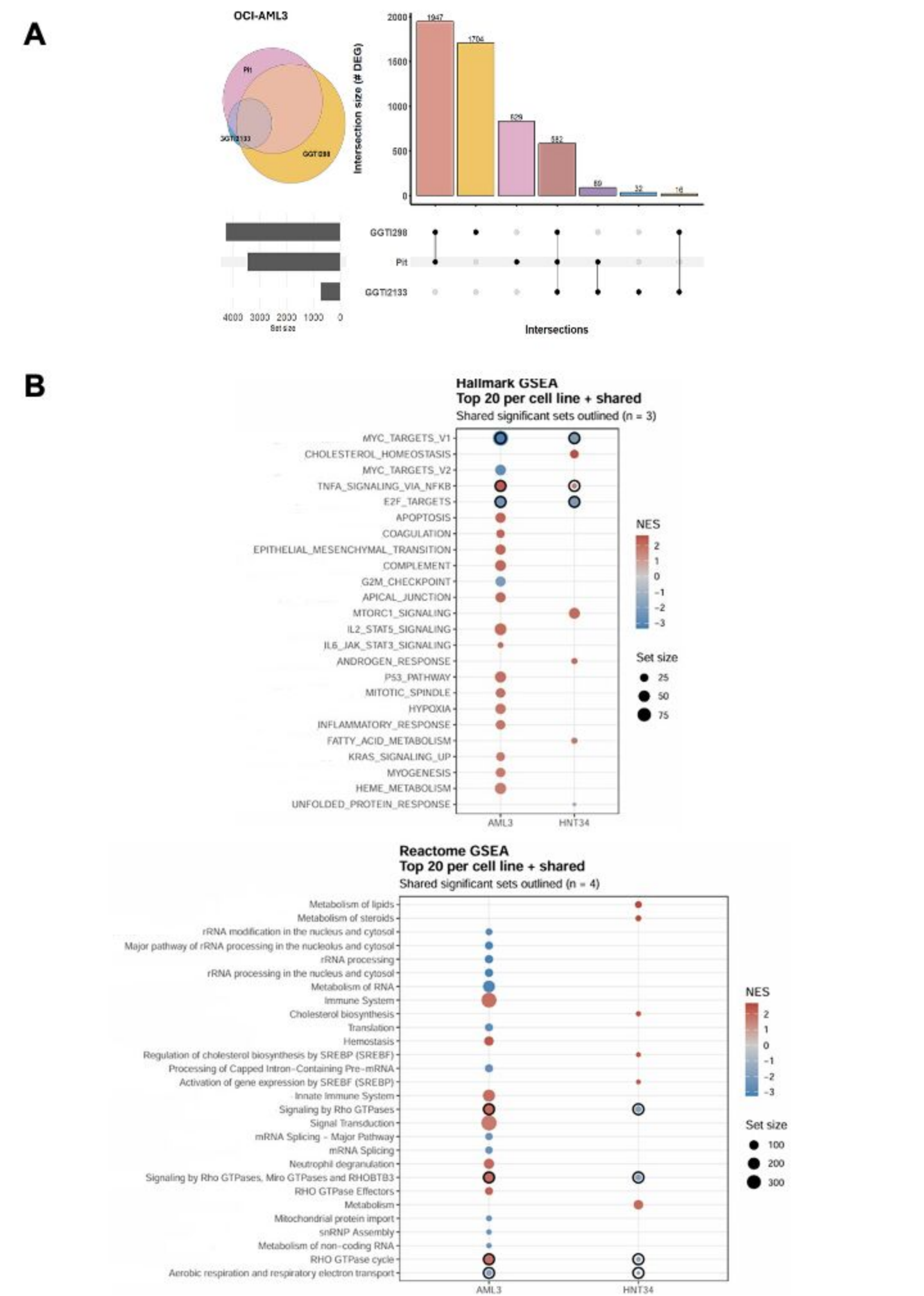
A
OCI-AML3
Pit
GGTI2133
GGTI298
Intersection size (# DEG)
2000
1500
1000
500
0
1947
1704
829
582
89
32
16
GGTI298
Pit
GGTI2133
4000 3000 2000 1000 0
Set size
Intersections
B
Hallmark GSEA
Top 20 per cell line + shared
Shared significant sets outlined (n = 3)
MYC_TARGETS_V1
CHOLESTEROL_HOMEOSTASIS
MYC_TARGETS_V2
TNFA_SIGNALING_VIA_NFKB
E2F_TARGETS
APOPTOSIS
COAGULATION
EPITHELIAL_MESENCHYMAL_TRANSITION
COMPLEMENT
G2M_CHECKPOINT
APICAL_JUNCTION
MTORC1_SIGNALING
IL2_STAT5_SIGNALING
IL6_JAK_STAT3_SIGNALING
ANDROGEN_RESPONSE
P53_PATHWAY
MITOTIC_SPINDLE
HYPOXIA
INFLAMMATORY_RESPONSE
FATTY_ACID_METABOLISM
KRAS_SIGNALING_UP
MYOGENESIS
HEME_METABOLISM
UNFOLDED_PROTEIN_RESPONSE
AML3
HNT34
NES
2
1
0
−1
−2
−3
Set size
25
50
75
Reactome GSEA
Top 20 per cell line + shared
Shared significant sets outlined (n = 4)
Metabolism of lipids
Metabolism of steroids
rRNA modification in the nucleus and cytosol
Major pathway of rRNA processing in the nucleolus and cytosol
rRNA processing
rRNA processing in the nucleus and cytosol
Metabolism of RNA
Immune System
Cholesterol biosynthesis
Translation
Hemostasis
Regulation of cholesterol biosynthesis by SREBP (SREBF)
Processing of Capped Intron-Containing Pre-mRNA
Activation of gene expression by SREBF (SREBP)
Innate Immune System
Signaling by Rho GTPases
Signal Transduction
mRNA Splicing - Major Pathway
mRNA Splicing
Neutrophil degranulation
Signaling by Rho GTPases, Miro GTPases and RHOBTB3
RHO GTPase Effectors
Metabolism
Mitochondrial protein import
snRNP Assembly
Metabolism of non-coding RNA
RHO GTPase cycle
Aerobic respiration and respiratory electron transport
AML3
HNT34
NES
2
1
0
−1
−2
−3
Set size
100
200
300

Figure 3

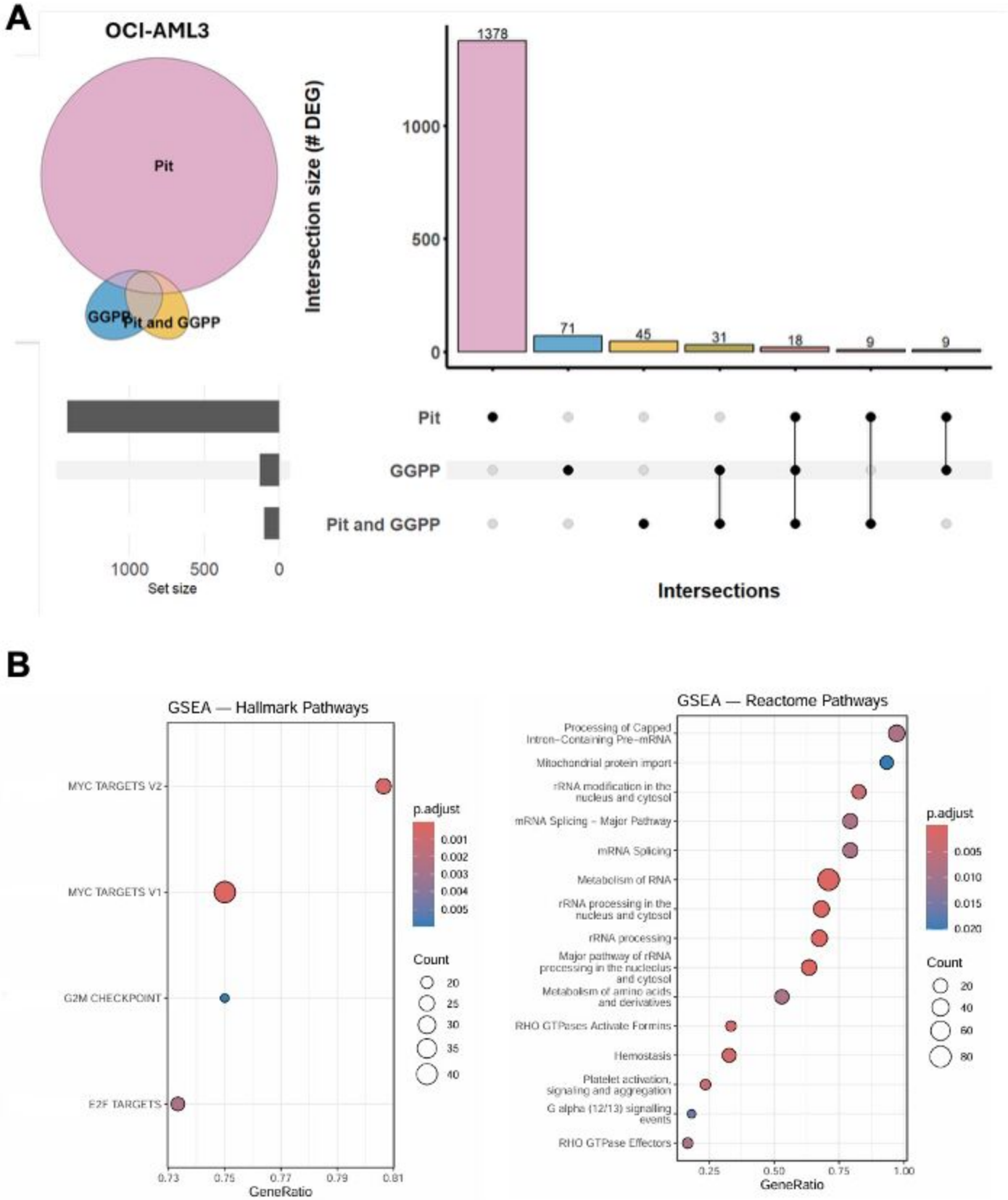
A
OCI-AML3
Pit
GGPP
Pit and GGPP
Intersection size (# DEG)
1378
71
45
31
18
9
9
1000
500
0
Pit
GGPP
Pit and GGPP
1000
500
0
Set size
Intersections
B
GSEA — Hallmark Pathways
MYC TARGETS V2
MYC TARGETS V1
G2M CHECKPOINT
E2F TARGETS
0.73
0.75
0.77
0.79
0.81
GeneRatio
p.adjust
0.001
0.002
0.003
0.004
0.005
Count
20
25
30
35
40
GSEA — Reactome Pathways
Processing of Capped Intron-Containing Pre-mRNA
Mitochondrial protein import
rRNA modification in the nucleus and cytosol
mRNA Splicing - Major Pathway
mRNA Splicing
Metabolism of RNA
rRNA processing in the nucleus and cytosol
rRNA processing
Major pathway of rRNA processing in the nucleolus and cytosol
Metabolism of amino acids and derivatives
RHO GTPases Activate Formins
Hemostasis
Platelet activation, signaling and aggregation
G alpha (12/13) signalling events
RHO GTPase Effectors
0.25
0.50
0.75
1.00
GeneRatio
p.adjust
0.005
0.010
0.015
0.020
Count
20
40
60
80

Figure 4

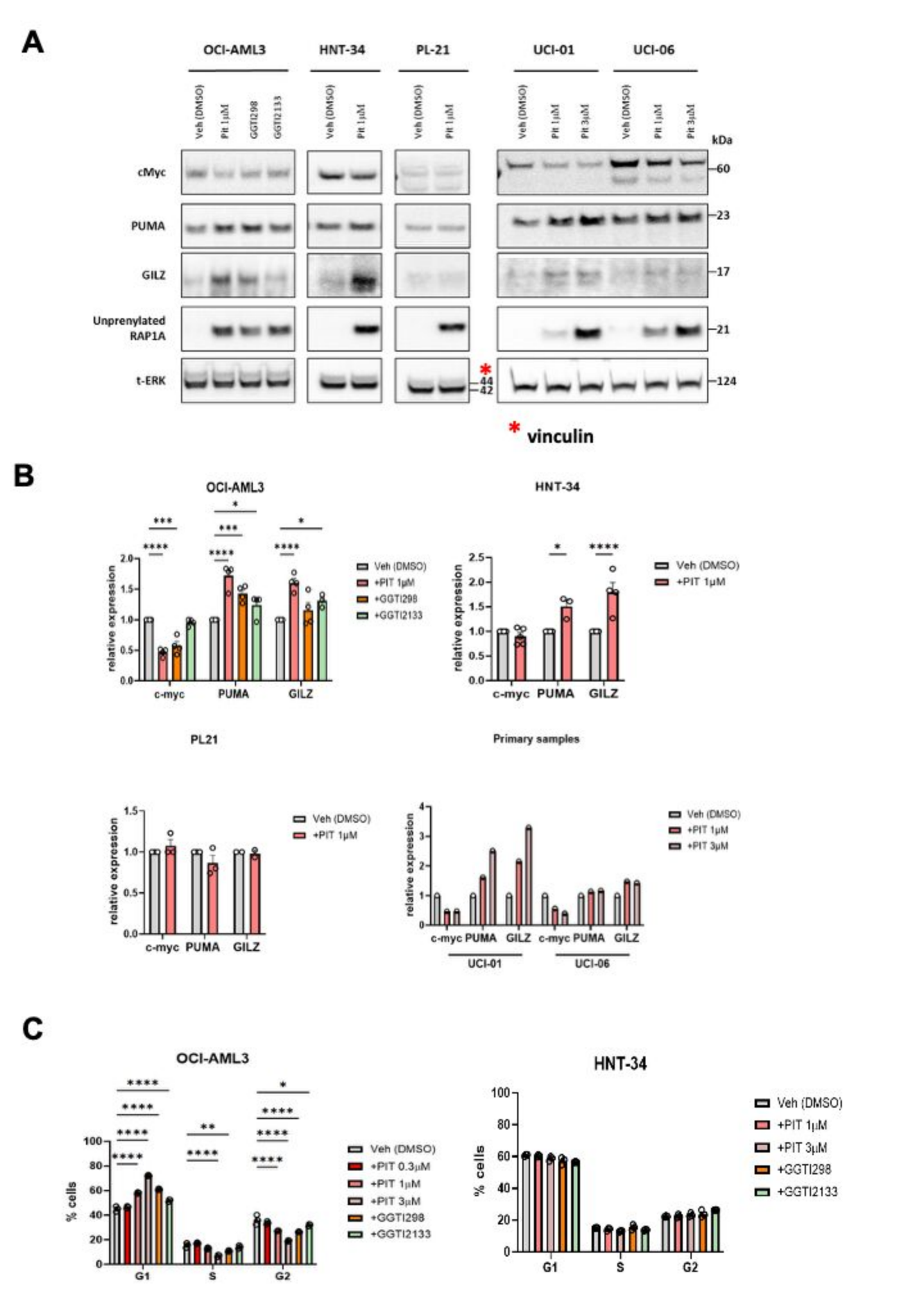
A
OCI-AML3
HNT-34
PL-21
UCI-01
UCI-06
Veh (DMSO)
Pit 1μM
GGTI298
GGTI2133
Pit 3μM
kDa
cMyc
PUMA
GILZ
Unprenylated RAP1A
t-ERK
60
23
17
21
124
44
42
* vinculin
B
OCI-AML3
HNT-34
PL21
Primary samples
relative expression
c-myc
PUMA
GILZ
Veh (DMSO)
+PIT 1μM
+GGTI298
+GGTI2133
+PIT 3μM
UCI-01
UCI-06
C
OCI-AML3
HNT-34
% cells
G1
S
G2
Veh (DMSO)
+PIT 0.3μM
+PIT 1μM
+PIT 3μM
+GGTI298
+GGTI2133

Figure 5

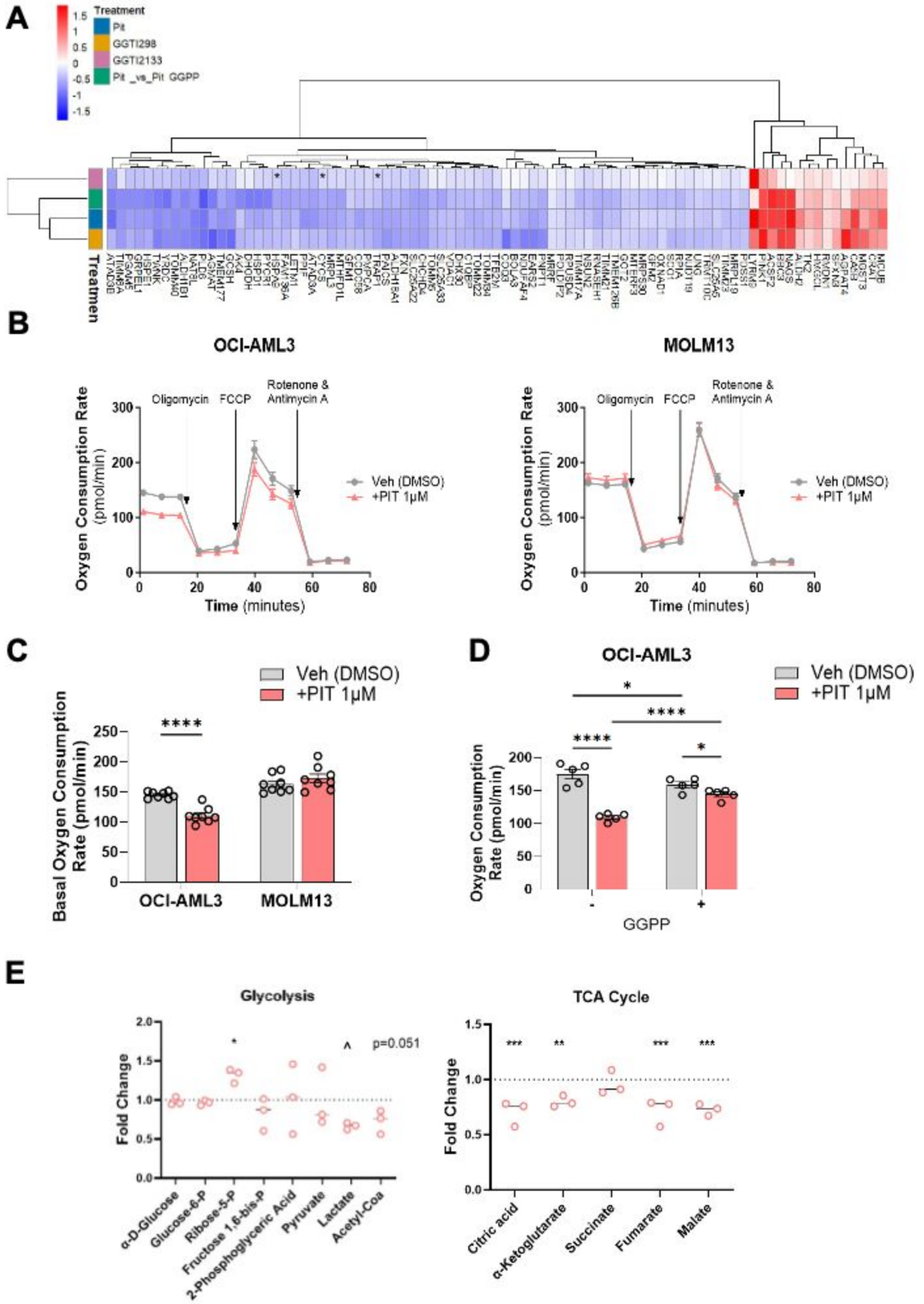
A
Treatment
Pit
GGTI298
GGTI2133
Pit _vs_Pit GGPP
Treatmen
B
OCI-AML3
MOLM13
Oligomycin
FCCP
Rotenone & Antimycin A
Oxygen Consumption Rate (pmol/min)
Time (minutes)
Veh (DMSO)
+PIT 1μM
C
Basal Oxygen Consumption Rate (pmol/min)
OCI-AML3
MOLM13
D
OCI-AML3
Oxygen Consumption Rate (pmol/min)
GGPP
E
Glycolysis
Fold Change
p=0.051
α-D-Glucose
Glucose-6-P
Ribose-5-P
Fructose 1,6-bis-P
2-Phosphoglyceric Acid
Pyruvate
Lactate
Acetyl-Coa
TCA Cycle
Citric acid
α-Ketoglutarate
Succinate
Fumarate
Malate

Figure 6